METHODS OF UTILIZING EARTH-ABUNDANT AND LUNAR MINERALS IN MATERIAL EXTRUSION-BASED ADDITIVE MANUFACTURING

by

Anna K. Hayes

A Thesis Submitted to the Faculty of the

DEPARTMENT OF MATERIALS SCIENCE AND ENGINEERING

In Partial Fulfillment of the Requirements

For the Degree of

MASTER OF SCIENCE

In the Graduate College

THE UNIVERSITY OF ARIZONA

2019

THE UNIVERSITY OF ARIZONA
GRADUATE COLLEGE

As members of the Master's Committee, we certify that we have read the thesis prepared by Anna Hayes, titled "Methods of Utilizing Earth-Abundant and Lunar Minerals in Material Extrusion-Based Additive Manufacturing" and recommend that it be accepted as fulfilling the thesis requirement for the Master's Degree.

Krishna Muralidharan Date: 8/9/19

Barrett G. Potter Jr. Date: 9 Aug 2019

Douglas A. Loy Date: 8/9/2019

Final approval and acceptance of this thesis is contingent upon the candidate's submission of the final copies of the thesis to the Graduate College.

We hereby certify that we have read this thesis prepared under our direction and recommend that it be accepted as fulfilling the Master's requirement.

Krishna Muralidharan Date: 8/9/19
Master's Thesis Committee Co-Chair
Department of Materials Science and Engineering

Barrett G. Potter, Jr. Date: 9 Aug 2019.
Master's Thesis Committee Co-Chair
Department of Materials Science and Engineering

ACKNOWLEGEMENTS

I want to thank all who supported me during the preparation of this thesis, without whose help I would not have been able to complete this work. First, my utmost gratitude goes to Dr. Douglas Loy, who had the vision to explore additive manufacturing in extraterrestrial environments and who directed the creation of this thesis. I am indebted to him as well as Dr. Krishna Muralidharan and Dr. B.G. Potter for their continued guidance in my research and beyond.

Thanks to Dr. Jessica Barnes and Dr. Moe Momayez, who provided perspective on the choice of minerals and contributed samples to support my work.

To everyone who I had the pleasure of working with in the lab – thank you for your assistance and fruitful discussions which helped my work to progress. Although this list is not all-inclusive, thanks to Dr. Sahila Perananthan, Anupama Pereis, Piaoran Ye, Lucas Sanders, and Pratish Rao. I am grateful to Susana Castillo for her friendship and support, without whom my time here would have been much less enjoyable.

Finally, thanks to my family and friends for all their encouragement. To Graham – thank you for always standing by me with love and patience.

TABLE OF CONTENTS

LIST OF TABLES

LIST OF FIGURES

ABSTRACT

Additive manufacturing methods have great potential for rapid production of parts and devices in remote areas with limited access to supply chains. This work examines the use of mineral resources for inexpensive and low-energy additive manufacturing. Silica, basalt, and Lunar regolith simulant (LRS) were processed for use as additive manufacturing feedstock in conjunction with polymeric binders. Mineral powders were chemically functionalized and combined with acrylonitrile butadiene styrene (ABS) at filler loadings up to 5 wt.% to create 3D printed structures using the fused deposition modeling (FDM) process. The mechanical properties of the resulting structures were characterized by tensile testing and analysis of fracture surfaces.

Alternatively, processed minerals were used to prepare inks for robocasting using Pluronic F127 hydrogels as a carrier. Minerals were added in increasing concentrations to determine the maximum filler loading that could be used to create an ink with suitable viscosity for the robocasting process. Hydrogels containing 52-57 wt.% mineral fillers were used as feedstock. By sintering the 3D printed green bodies, structural ceramics may be produced using this process. This work provides methods for producing structures and devices on demand in hostile environments through efficient *in situ* resource utilization.

CHAPTER 1: INTRODUCTION

Additive manufacturing (AM) and 3D printing of materials offers an exciting opportunity for rapid, agile production of parts and devices for a variety of engineering and technological applications. In particular, AM/3D printing (used synonymously) has become increasingly popular as it can create complex structures, reduce waste, and lower lead times of part production when compared to traditional manufacturing methods. Compared to subtractive manufacturing in which material is machined away to attain a desirable geometry, parts built using AM are typically produced in a layer-by-layer fashion in near-net shape. AM can also produce low volume parts much faster than manufacturing methods like injection molding or casting where the lead time to create a mold must also be considered. For this reason, AM was initially popular for prototyping although now its influence has grown into manufacturing of production parts.

In remote environments such as the battlefield, off-world bases, and humanitarian camps, the logistics of receiving parts becomes complicated and costly due to limited access to supply chains. Using AM equipment for on-site production provides flexibility to create a variety of geometries from a single source of raw material, which could be furthered by using *in situ* resources to decrease raw material and transportation costs. In this regard, this thesis examines the ability to manufacture structural prototypes in remote environments using available, native resources. In particular, simulants characteristic of the Lunar regolith and earth-abundant minerals will be assessed in terms of their compatibility with standard AM techniques.

1.1 Additive Manufacturing Processes

According to "History of Additive Manufacturing" in Wohlers Report 2016, the first AM technology to be commercialized by 3D Systems in 1987 was the Stereolithography Apparatus (SLA), in which a photosensitive polymer is cured by UV laser. In the 1990's several other technologies were commercialized including Fused Deposition Modeling (FDM™), Laminated Object Manufacturing (LOM), and Selective Laser Sintering (SLS). FDM technology exploded in popularity after inexpensive equipment based on the RepRap open-source project entered the market [1]. It is popular both in industry and with hobbyists due to its low cost, ease of use, and applicability to manufacturing a variety of thermoplastics. While all of the AM technologies that have been developed are far too numerous to list here, ISO/ASTM 52900-15 summarizes processes into the following categories [2]:

- **Material extrusion:** A material is deposited from an extruder onto a substrate.
- **Vat photo-polymerization:** A vat of photopolymer resin is exposed to an energy source which hardens the material layer-by-layer.
- **Material jetting:** Specialty printheads spray a liquid material onto a substrate.
- **Binder jetting:** A liquid bonding agent is deposited onto a bed of powder.
- **Sheet lamination:** Sheets of material are fused together, with the desired shape etched into each sheet.
- **Powder bed fusion (PBF):** An energy source is directed at a bed of powder to heat the individual particles until they fuse together.
- **Directed energy deposition (DED):** A metal powder or metal feedstock is fed in front of an energy source mounted on a multiaxis robotic arm.

Regardless of the manufacturing process used, AM production begins with a 3D model of the part that is created using computer-aided design (CAD) software or a 3D scan. Software is used to slice the 3D model into individual layers and create toolpath codes in a build or slice file. The model is then built according to the build file and the process specific to the machine. The choice of manufacturing process and machine determines the qualities of the finished part, including dimensional accuracy, surface roughness, mechanical properties, and structural anisotropy of the finished part introduced from the layer-by-layer processing method. Each process has advantages and disadvantages, as well as limitations in terms of the feedstock which can be used. Through the ever-growing options of materials and processes, AM has been used in applications ranging from aerospace components, to automobile parts, to medical implants, to human organs. To be cost-effective, AM is generally limited to complex or low volume production parts. However, AM has been found to be advantageous over other manufacturing methods in many cases by eliminating steps in production, for ease in building multi-material objects, or through enhancement of certain properties [3].

1.2 Manufacturing in Remote Environments

Introducing manufacturing equipment to field operations in remote environments allows for the design and production of parts to carry out repairs and to respond to problems as they arise. Lead times and transportation costs can be decreased dramatically by producing parts on site. AM is already being utilized by astronauts on the International Space Station, in Army field operations, and in humanitarian efforts.

Snyder et al. tested a commercial FDM 3D printer in low earth orbit and found that only minor adjustments needed to be made to the printer to successfully build parts in microgravity

[4]. Later NASA contracted Made in Space Inc. to design and build an FDM 3D printer to be used aboard the International Space Station [5]. In 2014, the 3D printer was launched and used to build 20 unique geometries. All were built successfully, including a part that failed on Earth due to sagging from gravity. NASA hopes to start producing all science equipment in space, as it can take months or even years for parts to reach space depending on launch resupply schedules.

The Army created the Expeditionary Lab – Mobile in 2012 to deploy as part of their Rapid Equipping Force in Afghanistan [6]. The lab is built in a standard 20-foot shipping container and holds an FDM 3D printer for plastic parts and a CNC machine for steel and aluminum parts. It allows soldiers to work directly with engineers to solve problems in the field and the full lab can be transported by truck or helicopter to where it is needed. The Army also has three Mobile Parts Hospitals that each contain a CNC and lathe [7]. In 2009, one of the Mobile Parts Hospitals produced over 11,000 critical replacement parts and in one case saved the Army an estimated $393,000 through the replacement of an Apache AH-64D rear rotor that would typically be done by sending the helicopter back to the U.S. for a rebuild.

The Army Research Laboratory is also exploring cold-spray technology for repairs and preventative maintenance of equipment in the field [8]. Cold-spray is a method of accelerating metal powder at supersonic speed onto a substrate. Although it was traditionally used for coatings or repair of preexisting parts, it has more recently been developed into a hybrid AM process, in which a part is produced in a rough near net shape then machined to the final geometry. Although the extra step of machining is necessary due to the low resolution of cold-spray, this hybrid method is still faster than other metal AM processes [9]. Currently, all the operations discussed use feedstock which must be carried to site.

The addition of *in situ* resource utilization could expand manufacturing capabilities in the field by further lowering transportation costs. This notion is especially powerful in AM processes in which feedstock can be prepared with minimal processing steps. Both native materials and material that is carried in but would otherwise be waste may be considered as *in situ* resources for AM feedstock. By using these resources and recycling components when they are no longer useful, a remote base could become almost entirely self-sufficient with AM equipment. Figure 1.1 provides a map of *in situ* resource utilization at an Army forward operating base that can easily be extended for application in other remote environments.

Plastic waste may be cut up, extruded into a spool of filament, and then used to 3D print a

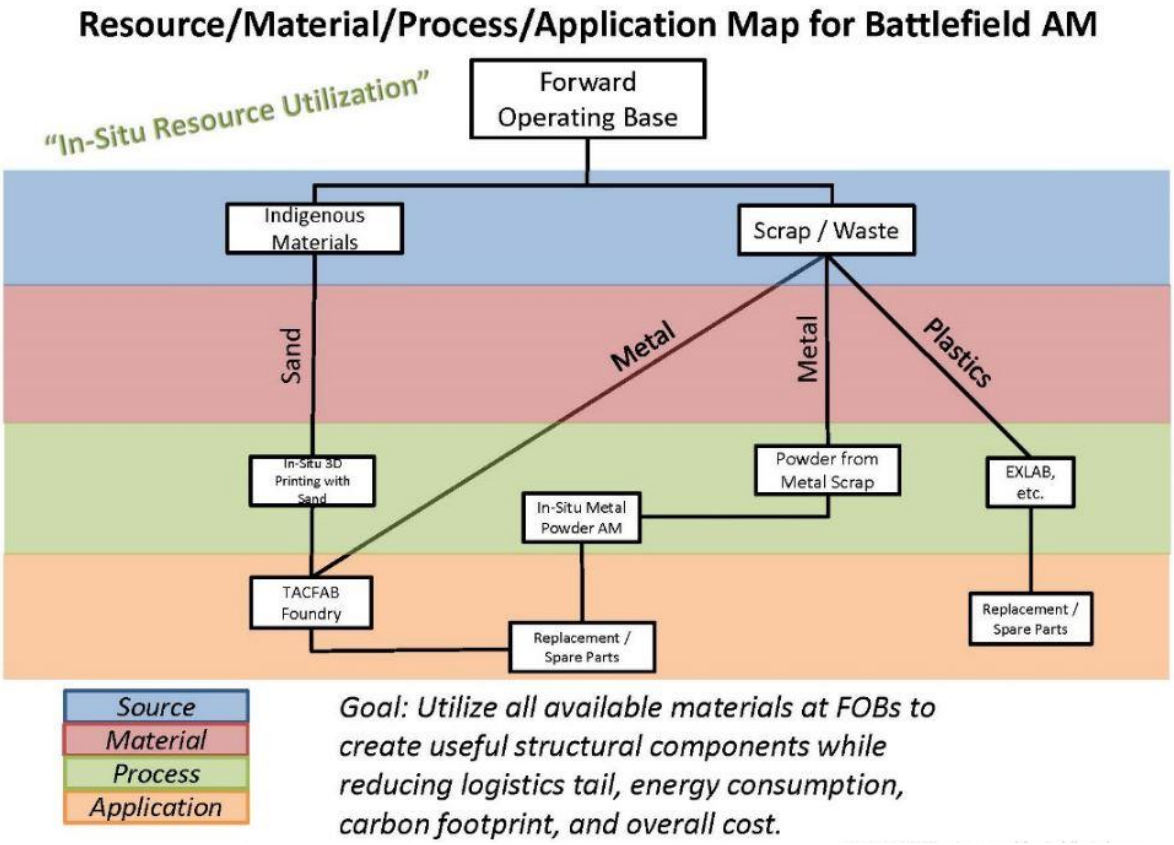

Figure 1.1. Map of in situ resource utilization at forward operating bases developed by the Army Research Laboratory, describing the use of indigenous materials and waste as AM feedstock [11].

new component using the FDM process. Recycling of thermoplastics has been studied extensively and shown to be possible while causing some degradation of the mechanical properties, so this would have to be considered when designing new components [10]. Benchtop recycling systems for pelletizing plastics are already being sold as part of the FDM workflow and could be readily transported to remote sites.

Recycling of metal parts to create powder or wire feedstock needed for PBF and DED processes would require much more intensive processing. Extracting metal from native minerals would also require well-established infrastructure. In the context of a mobile laboratory or in the early stages of space exploration, metal feedstock would likely be limited to scrap metal from machining operations that could be milled into a powder. As an alternative, Army Research Laboratory is exploring AM of native sand using a binder jetting process to create molds for metal casting [11]. This provides the capability of recycling metal parts in the field with the binder being the only material transported to site specifically for use in the process.

By far the most abundant *in situ* resource is native minerals, which can be used in their unrefined state as feedstock for composite and multi-component ceramic production. Milling and sieving would be the only processing steps necessary to collect a mineral powder. This powder could be used directly in high energy AM processes like PBF or DED or combined with a binder for application in several other AM processes.

To select an AM process compatible with *in situ* resources and to be used in a remote environment, certain considerations become important including: (1) environmental effects on the system and the system effects on the environment, (2) water and gas requirements, (3) form and storage requirements of feedstock, (4) level of training needed to operate the machine, and (5) maintenance [12]. Feedstock processing and part post-processing must also be minimized to

limit the footprint of a mobile fabrication laboratory.

Meisel et al. created a decision support framework to guide the selection of an AM process for use in a remote environment, providing the example of deploying the machine in a desert environment in support of soldiers [12]. The given constraints were typical to the needs of the Army: the machine would be contained in a Conex container, a large build envelope was required, and it would be operated by technicians with minimal technical training. Based on their tool, applicable processes in this situation would be material extrusion, binder jetting, and material jetting.

Sgambati et al. surveyed a wide range of AM technologies relevant to the creation of infrastructure, machinery, and commodities needed to a construct a lunar base [13]. They analyzed AM technologies based on capabilities, environmental conditions, power requirements, post-processing needs, and sustainability and found that FDM was the optimal technology to be used. FDM has been tested in microgravity, recycling of parts is possible, it produces minimal toxic fumes, and parts can used with little or no post-processing. The authors note that further assessment should be carried out for the materials that need to be brought from Earth to establish the process.

Given this support for *in situ* resource utilization in AM processes and the ability to adapt material extrusion processes to remote, including off-world, manufacturing, this thesis will focus on the use of abundant minerals in FDM and robocasting processes. FDM is a process that can be used for producing thermoplastics, in which minerals may be used as a filler. Robocasting is another material extrusion process traditionally used in ceramic processing, so a binder will be used to process minerals into feedstock. To explain the context and methods of this work, the remainder of the thesis will be arranged as follows: Chapter 2 will provide background on *in situ*

resource utilization in traditional and AM manufacturing methods, to further provide the motivation of this project. Chapter 3 will describe the experimental methods used for mineral processing and AM of structural components. Chapter 4 will discuss the results of utilizing *in situ* mineral resources as filler in acrylonitrile butadiene styrene (ABS) composites produced using FDM. Chapter 5 will focus on the use of *in situ* minerals in conjunction with a hydrogel carrier as feedstock in the robocasting process. Finally, Chapter 6 will provide a summary of the research findings and insight for future work in this area.

CHAPTER 2: BACKGROUND AND OBJECTIVES

In this chapter, a brief review of past and ongoing research efforts in the context of *in situ* resource utilization for manufacturing in remote environments will be provided. Given the overall thrust of this thesis as discussed in Chapter 1, the review will focus on the incorporation of recycled materials and native minerals for manufacturing of parts and prototypes with AM.

2.1 Background

Army Research Laboratory has proposed using AM to "bridge the gap" in the battlefield by building parts as a temporary replacement to keep systems operational while waiting for the arrival of the actual replacement [11]. A primary objective of this effort is to initiate the use of recycled and reclaimed materials to overcome the limitation of using proprietary filament feedstock. Plastic taken from food packaging and water bottles was recycled into 3D printed structures to be compared to structures printed from the proprietary ABS filament previously used. The polymers tested were polyethylene terephthalate (PET), polystyrene (PS), high density/low density polyethylene (H/LDPE), polypropylene (PP), and polycarbonate (PC). Each polymer presented unique challenges in the filament extrusion or printing process, with further optimization needed to achieve 3D printed parts of comparable quality to ABS.

Mohammed et al. demonstrated recycling of ABS, the plastic most commonly used as FDM feedstock and also found in electronic casings and car parts, to create 3D printed parts using only solar derived energy throughout the process [14]. Electronic waste was processed by a hand operated granulation device, extruded into filament, then used to 3D print complex structures. They established that their recycling process could be an effective humanitarian tool

with the successful fabrication of a pipe connector from recycled ABS without a degradation in print quality when compared to a part printed from virgin filament.

Much research on *in situ* research utilization in off-world manufacturing has been focused on the construction of large-scale infrastructure using native minerals found in the loose layer of regolith covering the Moon and Mars. The first step in establishing Lunar and Martian bases will be the construction of buildings for radiation shielding and roads for ease of transportation. Chow et al. found that Martian regolith simulant could be compacted into bricks with a strength of 30-50 MPa due to the presence of nanoparticulate iron oxides and oxyhydroxides acting as a bonding agent [15]. For dust mitigation on the Lunar surface, Hintze et al. used both solar sintering and the spraying of UV or heat curable polymers to create a thin layer of consolidated lunar regolith simulant (LRS) [16]. They chose solid, solvent-free polymers as binding agents to avoid potential difficulties from spraying liquid in a vacuum.

There has also been the development of specialized, large scale additive manufacturing methods for building construction. Meurisse et al. built a solar 3D printer for sintering LRS in a layer-by-layer fashion by the movement of a solar concentrator over a powder bed [17]. Bricks were produced with a compressive strength of 2.31 MPa, too low for use as a construction material. Further optimization of the process is needed to improve interlayer bonding and mitigation of thermal stresses. The method also needs to be tested in vacuum; however, it could be for producing radiation shielding if successfully implemented. Cesaretti et al. adapted the D-shape process to LRS [18]. The D-shape process is a large-scale binder jetting process in which an ink of salt water is jetted onto a powder bed of regolith. Upon mixing of powder and ink, magnesium oxide reacts with magnesium chloride in the chemical process that forms Sorel cement. Based on data from the Apollo missions, the authors determined that Lunar regolith has

sufficient magnesium oxide for this reaction. With evidence for water on the Moon, the only material to be brought from Earth would be the salts which make up 23 wt.% of the ink. This method produced structures with a compressive strength of 20 MPa.

However, these methods for large-scale manufacturing are not necessarily relevant for producing more complex commodity items that will be needed during the phase of human settlement to expand infrastructure and maintain equipment. Lunar and Martian regolith has also been explored as feedstock in typical AM processes. Crenshaw et al. used LRS in an ExOne inkjet printer to create multi-component ceramics with possible applications as radiation, humidity, and chemical sensors [19]. They successfully fabricated structures on Earth, but further testing must be carried out to determine the effect of microgravity on the binder jetting process. ExOne uses a proprietary solvent-based binder, so it may be assumed that this would need to be brought from Earth. The final parts were sintered to create ceramic structures.

Balla et al. demonstrated the use of LRS as a powder feedstock in DED [20], while Goulas et al. utilized Lunar and Martian regolith as feedstock in PBF [21], [22]. To prepare feedstock for the DED process, the regolith was first sieved to obtain powder with a size distribution of 50 to 150 μm. This was used to create dense Lunar regolith specimens, although further research must be carried out to characterize their mechanical properties. Laser PBF produced Lunar and Martian regolith simulant samples with bulk densities of 60% and 41%, respectively, due to low packing densities of the jagged, irregular powders. The regolith simulants were first prepared by sieving to a mean particle size of 70 μm. These high-energy AM processes enable the use of regolith as the sole feedstock component. Some post-processing equipment is needed to obtain a useable product, with the minimum being a machining process to remove the finished part from the baseplate and polish the baseplate for later use. Gas

requirements must also be taken into consideration. Goulas et al. produced parts under argon atmosphere, although it is not clear whether this would be necessary when using oxide powder as a feedstock.

Jakus et al. used solvent-based inks in robocasting, sometimes called direct ink writing (DIW), to create polymer composites containing 70% by volume Lunar or Martian regolith simulants [23]. Regolith simulants were first sieved to below 50 μm, then physically mixed with polylactic-co-glycolic acid copolymer dissolved in a solvent mixture of dichloromethane with 2-butoxyethanol and dibutyl phthalate additives. The hypothesis was based on the fact that dichloromethane would evaporate during ink synthesis and the printing process, with the solvent being collected to prevent adverse health conditions from prolonged exposure. The remaining 2-butoxyethanol and dibutyl phthalate would be collected from the printed parts by washing with ethanol and this mixture could then be distilled to obtain the constituents. The authors postulated that the polylactic-co-glycolic acid and dichloromethane may be synthesized from biological waste. With the establishment of chemical reactors and a solvent reclamation system, all the substances used in the process excluding ethanol would be produced from materials extracted from the Lunar or Martian environment, but the transportation and maintenance costs to establish this infrastructure should also be considered. Their process produces elastomeric structures which can be used as soft materials or sintered to create multi-component ceramics. In a later work, the authors sintered LRS-filled trusses at 1100°C in air and hydrogen [24]. The structures had compressive strengths ranging from 1 to 19 MPa regardless of the sintering atmosphere used, corresponding to relative densities of 18-43%. These values are comparable to compressive strengths of commercial ceramic foams.

From the literature review, it is apparent that there is lack of methods that utilize *in situ*

mineral resources in material extrusion-based AM processes, which are common and would be easily adapted to remote environments. Furthermore, preparation of the feedstock and the AM process should be carried out using portable equipment, have low energy requirements, and be safe if carried out in a confined environment. Meeting these requirements would allow for easy integration of the process to mobile and off-world manufacturing. The need for AM and *in situ* resource utilization will likely grow, considering NASA's announcement to establish a permanent lunar-orbit space station and begin lunar landings by 2024 [25]. In the immediate future, we can expect AM to be carried out with minimal infrastructure to support feedstock synthesis and processing both on Earth and the Moon. There are many benefits to creating a mobile fabrication laboratory in a small space like the shipping containers the Army is currently using, so it can be assumed that the AM will continue to be applied in this context.

It has been established that the most readily accessible resources in these environments to be used for AM feedstock are native minerals and recycled plastic. Recycled plastic has been found adequate to produce quality parts by FDM, albeit with a reduction in mechanical properties. Minerals are often added to polymers to enhance their properties and lower costs. In remote manufacturing, Earth-based or Lunar regolith minerals could be used as a filler in FDM filament to limit the amount of plastic needed to create parts and enhance their mechanical properties. It has not yet been determined how this addition will affect the mechanical properties of the resultant parts. Using LRS to create multi-component ceramic parts has been limited to high energy or solvent-based processes. In the early stages of development of a remote base on Earth, it can be assumed that water will be available to use as a solvent. The presence of water on the Moon has also been confirmed [26]. It will also be more complicated to implement AM technologies that use liquid or powder as a raw material as compared to material extrusion-based

technologies that use filament or a paste as feedstock. Therefore, there is a need to develop alternative methods that take these considerations into account.

While work from Mohammed et al. and others supports the use of FDM and recycled ABS in remote manufacturing, the work presented in this thesis will be the first application of Earth-abundant and Lunar minerals in their unrefined state as filler [14]. It will also provide an alternative, aqueous method of robocasting Earth-abundant and Lunar minerals to produce multi-component ceramics, as opposed to the solvent-based method developed by Jakus et al. [23]. In the following sections, a detailed discussion on the two AM methods that will be adopted in this will be given, in conjunction with methods used for processing of the raw materials that is required to make the materials feedstock amenable for AM.

2.1.1 Mineral Processing

The preparation of minerals may be through synthetic or direct processes. Synthetic methods can yield high-purity, regularly shaped minerals with very small particle sizes. However, only direct methods are considered in this work as the focus is on utilizing mineral resources already present in the environment. In direct production, ore containing a high amount of the mineral of interest is the starting material. The first step involves size reduction or comminution of the ore through crushing and grinding. The ground product is generally classified according to size by sieves, water elutriators, or classifiers. Typically, minerals are purified either to obtain the pure mineral or for metal extraction through flotation, gravity concentration, or magnetic or electrostatic concentration [27]. As this work aims to minimize processing and maximum the amount of *in situ* resources utilized, the only processing steps taken were grinding and classification to obtain a useable mineral mixture for later steps.

In preparation of polymer composites, previous work has shown that the chemical composition of the filler has little effect on the mechanical properties of the composite, while the morphology, size, and particle size distribution are important and affected by the grinding and classification steps [28]. Mineral composites typically use filler with a size of 0.5-10 μm, as even a small fraction of larger particles has been shown to be detrimental to strength and smaller particles may immobilize the polymer chains [29]. As an additional processing step, minerals may be coated with a compatibilizer. Surface modifiers are typically fatty acids, used as a processing aid, or organo-silanes that promote adhesion between the filler and polymer [29].

In preparation of powders for ceramic processing, chemical composition, size, size distribution, shape, and degree of agglomeration are important parameters. These factors will determine the powder packing and sinterability of the resultant artifacts. Processing of minerals for ceramics is usually focused on creating a homogenous powder with a narrow particle size distribution in the range of 0.1-100 μm [30].

2.1.2 Fused Deposition Modeling of Mineral Composites

Material extrusion technologies were first commercialized by Stratasys when they introduced FDM, also known as fused filament fabrication (FFF). Thermoplastic pellets are first extruded to form a spool of filament for feedstock. The filament is pushed through a heated nozzle attached to a gantry moving along a predetermined raster to form a layer. The plastic cools and solidifies rapidly so that this process can be repeated on subsequent layers as the bed moves further away from the nozzle.

The mechanical properties of FDM are anisotropic and inferior to those of an injection molded part. This is due to weak bonding between layers and raster lines. Failure of 3D printed

parts will occur along these areas and appear brittle when compared to a bulk specimen. Printing parameters like speed, nozzle size and temperature, and layer height will also have some effect on the mechanical properties as well as the quality of the part [31].

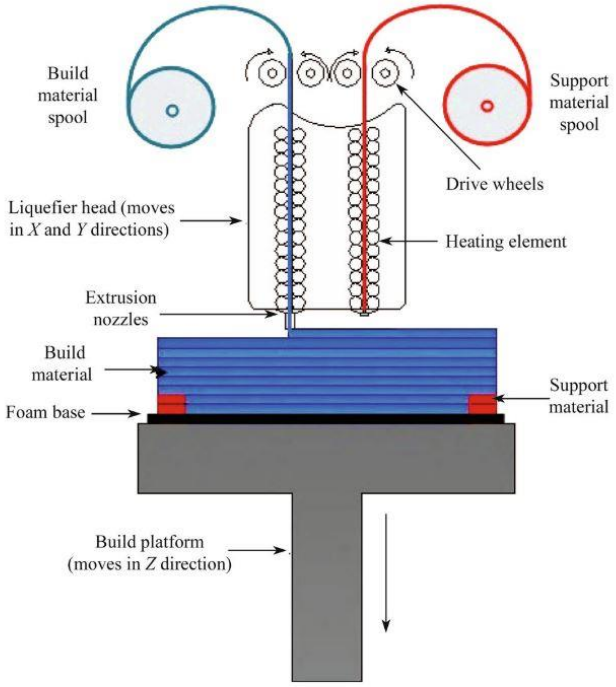

Figure 2.1. FDM process, in which thermoplastic filament is pushed through a heated extrusion nozzle by drive wheels [18].

Common thermoplastics used in FDM are acrylonitrile-butadiene-styrene (ABS), polylactic acid (PLA), and polycarbonate (PC), which are suitable to the process because they have relatively low melting points and melt viscosities that are low enough to enable extrusion and high enough to support upper layers while cooling [32]. FDM is generally limited to thermoplastics with a melting point of 300°C or less. Metals and ceramics can also be formed by this method by using polymer formulations that are highly filled with a ceramic or metal powder. This is sometimes called multiphase jet solidification or fused deposition of ceramics/metals. In this case, the part will be sintered to burn off the binder and form a dense ceramic or metal as the final product. More commonly, fillers are used in FDM to prepare composite materials.

As is the case with thermoplastic composites prepared by traditional manufacturing methods like injection molding, composites built using FDM may improve upon the mechanical properties of the polymer by increasing the strength, modulus, or toughness. Fillers, including mineral powders, are also sometimes added to thermoplastics to lower production costs. The

price of raw thermoplastics has dropped and now fillers generally serve to enhance to the polymer's properties or improve processability. Fillers may reduce mold shrinkage, increase the heat distortion temperature, improve UV resistance, and provide electrical and heat-insulating properties. Some common fillers are wood flour, clay, talc, fly ash, sand, mica, and glass beads [33].

Many varieties of composites common in traditional manufacturing have been explored for application to the FDM process. A number of composite filaments are sold commercially which contain fillers added to affect the mechanical, electrical, or magnetic properties of polymer, or for aesthetic reasons.

The greatest improvements in mechanical properties are seen in the use of continuous fiber reinforcement. Filament and 3D printer manufacturer Markforged produces Nylon filaments reinforced with continuous carbon, glass, or aramid fibers [34]. Their continuous carbon fiber filament has a tensile strength of 540 MPa, providing a dramatic increase in strength over their Onyx chopped carbon fiber filament (36 MPa) and unfilled Nylon filament (51 MPa) [35]. Both the Onyx and continuous carbon fiber filament also provide an increase in stiffness. Several other companies, including MatterHackers [36] and Formfutura [37], produce chopped carbon or glass fiber filaments for enhancements to the stiffness of the polymer, although the details of their polymer formulations are proprietary. Zhong et al. demonstrated the fabrication of 3D printed ABS containing up to 18 wt.% glass fibers [38]. They found that the composite filaments were too stiff to be 3D printed without the addition of a plasticizer and compatibilizer to improve processability. Ning et al. successfully incorporated 3-15 wt.% chopped carbon fiber into ABS, with 5 wt.% loading providing the maximum increase in tensile strength and 7.5 wt.% loading giving the greatest increase in elastic modulus [39]. Shofner et al. added 10 wt.% vapor

grown carbon fibers to ABS to increase the stiffness and tensile strength of 3D printed parts by 68% and 39%, respectively [40].

Composites containing fillers in the form of platelets have also been demonstrated to provide improvements to mechanical and other properties of the polymer matrix. Wei et al. produced ABS/graphene nanocomposites through chemical reduction of an ABS/graphene oxide dispersion [41]. The composites produced using this method could be used in the FDM process while containing up to 5.6 wt.% graphene, above which print failures became common, and had improved electrical conductivity and thermal stability. Dul et al. characterized the mechanical properties of 3D printed ABS/4 wt.% graphene composites produced by melt compounding and found the parts had an increased elastic modulus but lower tensile strength compared to pure ABS [42]. Weng et al. produced ABS composites containing 5 wt.% montmorillonite clay which provide an increase in strength and modulus [43]. They also found that the addition of clay filler lowered the coefficient of thermal expansion of the composite, leading to less warping during the printing process. PLA/clay composites were demonstrated by Coppola et al., who found that the addition of 4 wt.% filler led to an increase in elastic modulus and decrease in strength of the printed parts [44].

Particulate composites, containing metal, ceramic, or wood powders, are often used in FDM to produce parts for specific applications. Commercially, metal-filled filaments are advertised for their conductive or magnetic properties, as well as for aesthetic reasons. Similarly, wood and ceramic-filled filaments can be used to produce 3D printed part with unique capabilities for post-processing, including CC Products's Layceramic filament which can be fired like a ceramic [45]. Major companies producing specialty filaments include MatterHackers [36], Formfutura [37], colorFabb [46], and Proto-pasta [47]. While exact polymer formulations

are not given, the strength of highly-filled filaments is usually less than that of the base polymer, while modulus is higher. For example, Formfutura's StoneFil™ is a PLA-based filament containing about 50 wt.% powdered stone. The tensile strength is given to be 38.0 MPa and the elastic modulus is 4760 MPa [48], compared to values given for pure PLA of 56.6 MPa and 3368 MPa, respectively [49].

Many groups have explored the use of fillers in FDM to produce polymer composites for specific applications. Nikzad et al. produced ABS composites containing up to 40 vol.% iron or copper powder for the application of 3D printing injection molding inserts and found that the strength of the composites dropped dramatically with filler loading, but that the needed thermal properties were met [50]. Boparai et al. used FDM to fabricate Nylon-6/Al/Al_2O_3 composites containing 40 wt.% inorganic filler with improved wear resistance [51]. In order to use FDM to prepare composites with spatially varying permittivity, ceramic perovskite powders have been added to ABS in amounts up to 30 vol.% [52], [53]. For radiation shielding, Shemelya et al. added 0.33 vol.% tungsten powder to PC without affecting the tensile strength [54], while Woosley et al. created ABS composites containing up to 20 wt.% boron nitride which led to a reduction in tensile strength [55]. Kalita et al. created polypropylene/tricalcium phosphate filaments that may be used to create bone scaffolds with controlled porosity [56]. They found it necessary to introduce a wax and plasticizer to aid in processability, with the 3D printed composites exhibiting a tensile strength of 8.2 MPa compared to 19.8 MPa for pure polypropylene.

To determine the effect of particulate fillers on the mechanical properties of ABS parts produced using FDM, Torrado et al. added either 2 or 5 wt.% of MayaCrom© blue dye, TiO_2, ZnO, $SrTiO_3$ or Al_2O_3 to ABS [57]. Each filler caused a reduction in tensile strength, although in

some cases there was a decrease in anisotropy of the mechanical properties based on build direction. It was generally found that the filler particles acted as stress concentrators, causing the ABS to fail at lower stress and resulting in more brittle failure. Skorski et al. created ABS/TiO_2 composites containing 1-10 wt.% filler loading and found there was a slight increase in tensile strength in the 5 wt.% composite [58]. There has been limited research on the use of particulate mineral fillers in FDM and the effect processing, particle morphology, and particle size have on the mechanical properties of composite parts. Although Formfutura's StoneFil™ filament demonstrates the use of powered stone as filler, the effect on the mechanical properties of the polymer has not been well explored. This work will consider minerals and stones that have undergone minimal processing as filler, to determine the feasibility of utilizing *in situ* resources.

Factors influencing how fillers will affect the mechanical properties of a polymer include the morphology and size of the filler, filler/matrix interfacial adhesion, and filler loading. Fillers with a high aspect ratio like clay, glass fibers, and carbon nanotubes have been explored extensively because adding a small amount can provide a dramatic increase in mechanical properties. Inorganic fillers with an aspect ratio close to one or particulate fillers, although less popular, will also affect the mechanical properties of a polymer.

The elastic modulus of particulate filler/polymer composites is primarily dependent on the particle loading. Because minerals have a much higher elastic modulus than the polymer, the addition of a rigid phase will increase the stiffness of the polymer regardless of the size of the particulate or degree of adhesion [28]. The modulus of a glassy polymer containing a rigid particulate filler can be estimated by the Halpin-Tsai equation:

$$\frac{M}{M_m} = \frac{1 + AB\phi_f}{1 - B\psi\phi_f} \quad (1)$$

where M is the modulus of the composite, M_m is the corresponding modulus of the unreinforced matrix polymer, A is a constant that depends on the filler geometry and the Poisson's ratio of the matrix, ϕ_f is the volume fraction of filler, ψ is the maximum packing volume fraction of the filler, and B is a function of A and the relative modulus of the filler and matrix [33].

An increase of strength in the particulate/polymer composite depends on the mechanism of stress transfer to the filler. Smaller particles have been found to provide increases in strength due to a large surface area for stress transfer to occur. Improved particle/matrix adhesion provided by surface treatment of the filler will also give an increase in strength. The relationship between particle loading and strength is generally found to increase to some point beyond which the strength begins to decrease. This is because effective load transfer is dependent on good dispersion of the filler, which becomes increasingly difficult with higher loading. The relationship between the ultimate strength of a particulate-filled composite compared to the ultimate strength of the unfilled matrix can be represented by an equation proposed by Schrager:

$$\sigma_u = \sigma_m e^{-r\phi_f} \tag{2}$$

where σ_u is the ultimate strength of the composite, σ_m is the ultimate strength of the unfilled matrix, and r is an interfacial factor [33].

Toughness of the composite has been found to be dependent on the filler being smaller than a critical size, but with toughness increasing with increasing particle size. In polypropylene/calcium carbonate composites, treatment of the filler to increase adhesion has been found to increase the toughness [59]. However, other systems have shown a decrease in toughness with surface treatment of the filler. Similarly, toughness has been shown to either increase or decrease with an increase in particle loading. Although toughness is significantly

affected by particle/matrix adhesion and particle loading, trends vary between systems. Generally, the toughness of brittle polymers will increase with an increase in particle/matrix adhesion and particle loading, while ductile polymers lose toughness with an increase in particle adhesion and loading. Various mechanisms of toughening in particulate-polymer composites have been proposed including crack pinning, particle-matrix debonding, diffused matrix shear yielding, micro-cracking, and breakage of particles. It is possible that the mechanism of toughening varies dramatically between systems and may occur concurrently, hence the lack of definite trends [28].

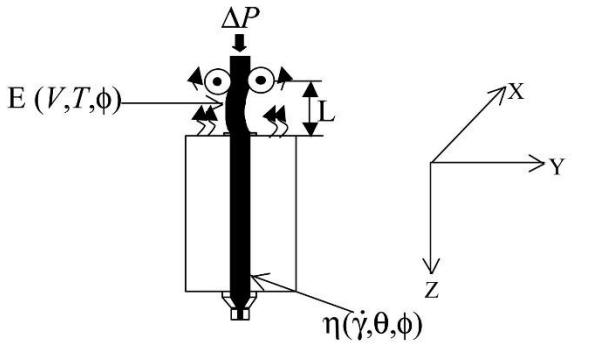

ΔP: Extrusion Pressure, V: Filament feed rate,
T, θ: temperature, ϕ: solids loading, γ̇: shear rate,
η: viscosity of feedstock, E: compressive stiffness of filament

Figure 2.2. Failure due to filament buckling in the liquefier during FDM process and relevant material and build parameters [23].

Mineral fillers will also affect processing procedures as they generally raise the melt viscosity of the polymer. The magnitude of this increase will depend on the shape, size distribution, and surface properties of the particles [29]. In FDM, this must be considered during both filament extrusion and the printing process. Filaments are acting as a piston during the FDM process and will buckle in the liquefier if the extrusion pressure exceeds a critical buckling stress, as shown in Figure 2.2. Venkatamaran et al. determined that buckling will occur if:

$$\frac{E}{\eta_a} < \frac{8Ql(L/R)^2}{\pi^3 r^4 k} \tag{3}$$

where E is the compressive modulus of the filament, η_α is the apparent viscosity as measured by a capillary viscometer, Q is the volumetric flow rate, l and r are the length and radius of the capillary, L and R are the length and radius of the filament in the liquefier, and k is a scaling

factor between the capillary and FDM extrusion pressure [60]. This equation establishes that a balance between stiffness and viscosity must be accomplished for filaments to be used successfully in the process. Process parameters such as nozzle temperature, geometry, and print speed will also need to be optimized to successfully print filled filaments.

2.1.3 Robocasting of Ceramics

Robocasting, also known as direct ink writing (DIW) or paste printing, is another technology in the material extrusion category but is distinct from thermoplastic extrusion processes. When first developed at Sandia National Laboratories in 1996, formulations consisted of colloidal aqueous slurries of ceramic powder that were printed onto a hotplate to quickly dry into a solid mass [61]. The process has been used extensively to produce oxide, carbide, and

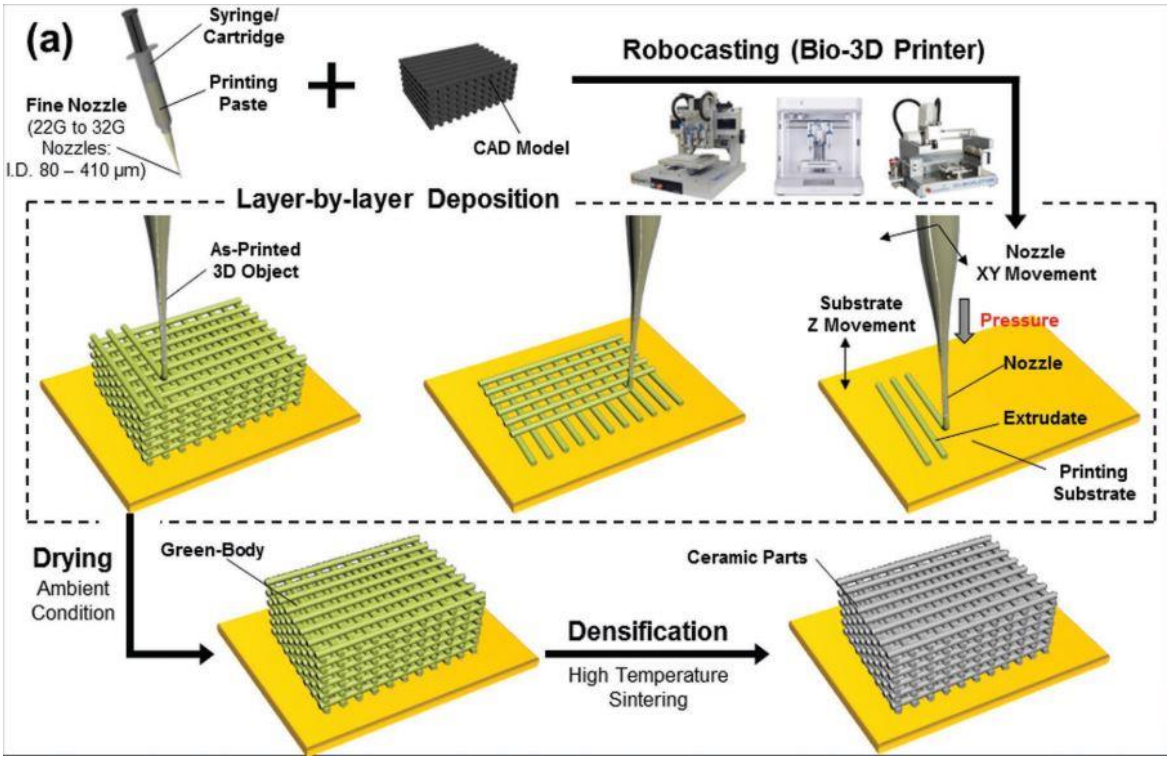

Figure 2.3. Robocasting process, in which a filled ink is extruded from a syringe through a nozzle to create a 3D green body that can later be sintered into a dense ceramic part [21].

nitride structural ceramics, functional ceramics, and glass scaffolds [61]–[65]. Robocasting formulations that have been developed since usually use inks composed of powder combined with a solvent and a small amount of organic additive. There are three general methods to stabilizing the ceramic powder in the ink formulation: (1) electrostatic, (2) steric, or (3) combined electrosteric. Electrostatic or electrosteric stabilization may use a polyelectrolyte aqueous ink, while steric stabilization usually uses a nonaqueous solvent or a hydrogel in the ink formulation. The powder must be well dispersed to achieve even extrusion and to avoid aggregates clogging the nozzle. The ink is deposited by a syringe attached to a moving print head layer by layer to form a three-dimensional object.

Concentrated inks used in robocasting must have suitable viscoelastic properties to be successfully printed, as described using the Herschel-Buckley model:

$$\tau = \tau_y + K\gamma^n \tag{4}$$

where τ is the applied shear stress, τ_y is the yield stress, K is the viscosity parameter, γ is the applied shear rate, and n is the shear thinning exponent. The criteria the ink must meet to be used successfully in the robocasting process is: (1) reversible shear-thinning behavior to a viscosity of 10-100 Pa s at high shear rate to facilitate extrusion while retaining shape after deposition and (2) sufficiently high modulus with a yield stress greater than 200 Pa to support subsequent layers without collapsing. Shear-thinning behavior also allows for lines to bridge over empty space. The choice of nozzle size and print speed will affect the resolution of the printed structure, but also the extrusion pressure needed. High viscosity formulations will require an increased extrusion pressure. Parameters like the print speed, line width, and layer height must also be optimized so that the extrudate is not stretched or discontinuous and lines fit

within each other to create a fairly dense structure [63].

After the printing process is complete, the part is dried, then heated to burn out the binder and sinter the powder particles to create the final dense structure. High powder loading is needed in the robocasting feedstock to prevent cracking or excessive shrinking during these subsequent steps. Binder burnout is carried out at a comparatively lower temperature, but high enough for the decomposition of all organic additives. Sintering is carried out to remove much of the pore space that will exist after the removal of the binder, although the robocasting process does result in some pores due to lack of filling between printed lines and layers. Densification via sintering is a thermodynamically favorable process as it lowers the interfacial energy the particles in the system. The sintering process is dependent on temperature, time, pressure, atmosphere, and heating and cooling rate. It is easier to achieve a dense structure if the powder used is homogeneous and has a high packing density [30].

2.2 Objectives

Having provided a background on the underlying issues concerned with *in situ* resource utilization in remote environments, and the relevance of implementing FDM and robocasting methods for such purposes, the specific objectives of this thesis are defined below.

The scope of the present work is to determine the feasibility of creating abundant mineral composites using FDM and hydrogel mineral-filled inks for robocasting. To provide a pathway for *in situ* resource utilization in AM, it is necessary to test the viability of incorporating unrefined minerals into these processes and to evaluate the mechanical properties of resultant parts. Silica, the most abundant mineral on Earth, will first be explored as a control. Basaltic stone will be used to represent a mineral mixture that would be encountered *in situ* and to

determine the level of processing needed to prepare AM feedstock. Basalt is found in any location with volcanic activity, which includes much of the Earth as well as the Moon and Mars. Finally, LRS will be used to determine the applicability of the processes to a Lunar base. The feedstock formulations should be insensitive to the chemical composition of the mineral filler, such that the same system could be used with regolith taken from a different location. This work will focus on processes to create feedstock and manufacture parts that can be carried out in a small and confined environment. Prepared feedstock in the form of filaments or ink can be processed separately from the AM equipment and stored until needed. With an understanding of the viability of using *in situ* resources in material extrusion-based AM and the properties of resultant parts, applications may be identified to potentially replace current methods of manufacturing and supply chains in remote environments. To summarize, the objectives of this work will be to:

1. Determine the feasibility of using earth-abundant minerals and LRS as filler for FDM feedstock.
2. Evaluate the relationship between mineral filler loading, surface treatment, and mechanical properties of acrylonitrile-butadiene-styrene (ABS) composites.
3. Develop a method of robocasting earth-abundant minerals and LRS to prepare green body multi-component ceramics.
4. Determine the maximum *in situ* resource utilization possible in robocasting hydrogel inks using the developed method.
5. Make recommendations for expeditionary forces and future space exploration.

CHAPTER 3: EXPERIMENTAL METHODS

In this chapter, the experimental procedure adopted for the fabrication of prototypes that incorporate materials characteristic of geo and lunar minerals is given.

3.1 Powder Processing and Characterization

The powder feedstock used in this work were silica, basalt, and LRS. The basalt and lunar regolith samples required sieving and grinding to obtain a powder of suitable size for use in AM. The silica powder was purchased from Alfa Aesar with an average particle size of less than 10 μm and used as received. The silica powder composition was similar to that of sand with a purity of >95 wt.% silica.

The basalt used in this work was a sample from Hawaii kindly donated by Dr. Momayez in the Department of Mining and Geological Engineering, at the University of Arizona. The elemental composition of the basalt was determined using a TM3000 scanning electron microscope (SEM) equipped with an energy dispersive x-ray spectrometer (EDS) and can be found in Table 3.1 below.

Table 3.1: Basalt Elemental Composition

Element	Weight (%)
Oxygen	49.8
Aluminum	17.5
Silicon	13.2
Barium	8.2
Iron	6.2
Fluorine	3.1
Calcium	2.0

Total	100

Several simulants of Lunar regolith have been developed from resources on Earth to aid in scientific research. For this work, LMS-1 was purchased from the Exolith Lab at University of Central Florida, which was created to simulate the mechanical properties of lunar regolith [66]. The chemical composition, as measured by X-ray fluorescence (XRF) and provided by the Exolith Lab, is given in Table 3.2 below [66]. Figure 3.1 shows optical images of the materials as received.

Table 3.2: LMS-1 Chemical Composition

Element	Weight (%)
SiO_2	46.0
TiO_2	1.3
Al_2O_3	12.9
Cr_2O_3	0.1
FeO_T	14.8
MgO	16.5
CaO	5.4
Na_2O	2.1
K_2O	0.6
SO_3	0.2
Total	100

The basalt and LRS samples were used with the minimum amount of processing required to create powders that could be applied to AM processes. The basalt sample was first crushed to obtain fragments with a size of about 10 mm or less. The crushed basalt and LRS were ground and sieved to obtain a powder of suitable size. Grinding was done using a Columbia International Vivtek planetary ball mill with agate jars and balls, shown in Figure 3.2. This lab

Figure 3.1. Images of **(a)** silica powder, **(b)** basaltic stone, and **(c)** LRS, as received.

scale ball milled is housed in the Lithe Integrated Agile Manufacturing (LIAM) lab and used for powder processing and AM feedstock preparation. The high-speed planetary motion produces centrifugal force that can rapidly produce a powder as fine as 0.1 µm through grinding between the balls and the wall of the jar. A small amount of deionized water was added before grinding, as the powder tended to aggregate on the side of the jar if ground while dry. Every 6 hours the slurry was removed from the jars and sieved, with coarse particles being returned for further milling. The usable slurry was classified by sieving through 180 µm and 45 µm meshes, followed by filtering through a polyethylene fritted funnel with 10 µm pore size. Samples were dried overnight at 100°C before further use.

After processing was complete, the morphology of each powder was characterized using scanning electron microscopy (SEM). Micrographs were taken using a Hitachi TM4000Plus tabletop microscope, which is part of the materials characterization equipment in the Department of Material Science and Engineering at the University of Arizona. In this SEM, a tungsten filament is

Figure 3.2. Lab-scale planetary ball mill used for powder processing.

heated to produce an electron beam which interacts with the sample to produce a signal of secondary or backscattered electrons. As the powders are insulating, they were first sputter coated with a 4 nm layer of gold. The images were taken at an operating voltage of 15 kV and collected with the backscattered electron detector to achieve high resolution images.

Dynamic light scattering (DLS) is a technique used to determine the particle size distribution, which is accomplished by shining a laser through a dispersion and measuring fluctuations in scattering intensity caused by Brownian motion of the particles. DLS measurements of the processed powders were taken using a Malvern Panalytical Zetasizer Nano ZSP, with access to the instrument being kindly provided by Dr. Reyes Sierra. This instrument uses a He-Ne laser light source operating at 633 nm and is sensitive to particles in the range of 0.3 nm to 10 μm. Dispersions were prepared by adding powder at a concentration of 0.005 vol.% to 100 mM KNO_3 solution which had been filtered through a 0.20 μm PTFE filter, before sonicating to break up aggregates and produce a nearly clear dispersion. Refractive index values were taken from literature and were 1.55 at a wavelength of 589 nm for silica [67], 1.52 at 647 nm for basalt [68], and 1.50 at 589 nm for LRS [69]. An absorptivity of 0.01 was used for each sample. The reported results are an average over 3 scans.

3.2 Fused Deposition Modeling

In selecting a thermoplastic for to use for mineral composites, ABS and PLA were the first considered as they are the most commonly used in FDM. For this reason, proper printing parameters and environment [70], as well as resulting mechanical properties [49], have been well-documented. Initial trials to create composite filaments were carried out for both plastics. A preliminary study showed the addition of mineral fillers increased the brittleness of filaments,

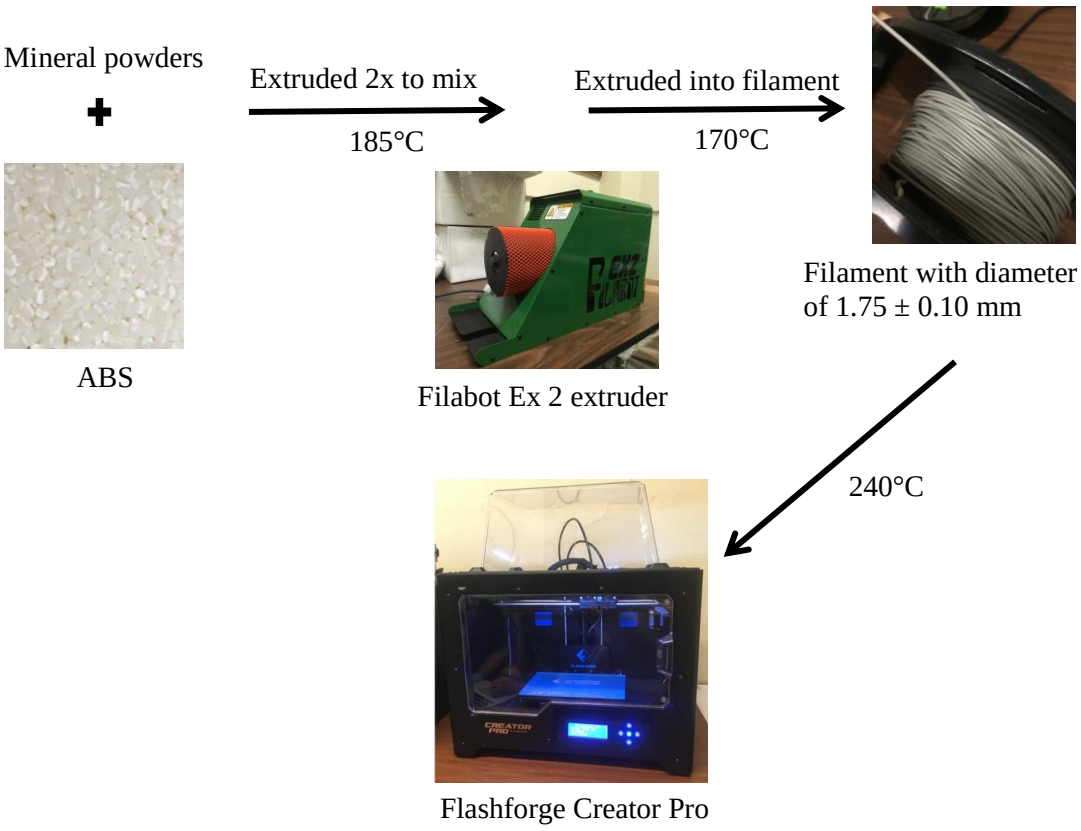

Figure 3.3. Procedure for preparing and 3D printing ABS composite filaments.

with this effect being more pronounced in PLA. Ultimately, ABS was used for the remainder of this work. ABS is also more commonly used in industry outside of 3D printing, which would give this work more significance if it is extended in the future to using recycled thermoplastics.

In some cases, mineral filler was treated by silane or stearic acid to determine the effect of filler-polymer adhesion on the mechanical properties. Silica powder was silane functionalized by adding 25 mg of N-(2-aminoethyl)-2,2,4-trimethyl-1-azasilacyclopentane to 5 g of silica in a sealed vial. The vial remained sealed for 2-3 days while a vapor phase reaction took place. After this time, the silica displayed hydrophobic behavior and excess silane was removed using a rotary evaporator in a water bath heated to 55°C. Alternatively, 3 g of silica powder was combined with 3 mg of stearic acid and ball milled for 3 hours. The heat generated during the

ball milling process was sufficient to melt the stearic acid and form a coating over the silica particles, as could be observed by the hydrophobic behavior of the powder.

To prepare ABS composite filaments, the respective mineral fillers were first mixed by hand with ABS pellets purchased from Filastruder. Mixing and extrusion of composite filaments was done on a Filabot EX2 single screw extruder in the LIAM lab. Neat ABS filament was also prepared following the same procedure to provide a baseline. The procedure for preparing filaments is illustrated in Figure 3.3. The procedure involved the extrusion of the ABS and filler mixture at 185°C. The resulting filament was cut up using wire cutters to pellets of about 3 mm in size and extruded once again at 185°C for further mixing. After being cut up to pellets, this filament was then extruded at 170°C onto a rotating spool, resulting in a total of 3 successive extrusion steps to aid in the development of a uniformly distributed filler phase. The speed of the spooler and the extruder could be adjusted to give filament with the proper diameter of 1.75 ± 0.10 mm.

The thermophysical properties of the prepared filaments were characterized using a TA Instruments DSC25 differential scanning calorimeter (DSC) in the materials characterization facilities. The glass transition temperature (T_g) of the filaments was found by heating a pan containing a sample alongside an empty reference pan. The glass transition temperature is seen as an inflection point on the graph of heat flow versus temperature, caused by a change in the sample's heat capacity. Filament samples weighing 3-5 mg were placed in a sealed aluminum pan and heated from 30°C to 120°C at rate of 10°C/min. The nozzle temperature used in the FDM process must be well above the glass transition or melting temperature of the polymer to achieve a melt of sufficiently low viscosity to extrude from the nozzle at the speed and pressure used in the process [71].

Filaments were 3D printed using a Flashforge Creator Pro equipped with an acrylic enclosure in the LIAM lab. Slic3r, an open source slicing software, was used to define the printing parameters and toolpaths [72]. The printing parameters were optimized by trial and error and visual inspection of printed parts to create dense structures and eliminate warping.

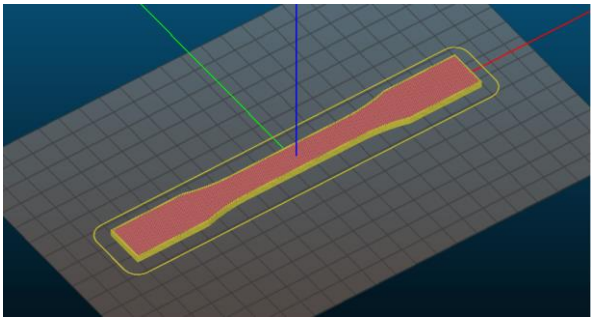

Figure 3.4. Slice file showing the build orientation of tensile test specimens.

Tensile testing of 3D printed samples was carried out on an MTS Criterion Model 42 equipped with a 5 kN load cell in the Mechanical Testing Laboratory in the Department of Materials Science and Engineering. The tests were conducted according to ASTM D638, at room temperature with a strain rate of 5 mm/min [7]. A minimum of 5 standard Type I specimens were 3D printed using the optimized printing parameters. Specimens were printed flat on the bed, as shown in Figure 3.4, and tested perpendicular to the build direction. The filament was laid down at alternating angles of 0° or 90° relative to the direction of applied tensile stress. Load and displacement data were collected. Fracture surfaces of the broken tensile specimens were analyzed using SEM.

3.3 Robocasting

A polymer solution is typically used as the carrier of powders used in robocasting inks, to impart a desirable viscosity and shear-thinning behavior. In selecting a polymer to be used in this project, the goals were to create an aqueous system that is not sensitive to changes in the chemistry of the powders. Hydrogels stabilize powders through steric interactions, therefore the rheological properties of the resultant ink are mainly depended on the particle fraction and

packing density rather than surface chemistry [73]. With this in mind, Pluronic F127 was selected for preparing mineral-filled hydrogel inks, which has been previously explored for robocasting both oxide and carbide powders successfully [62]. Pluronic F127 is a nonionic triblock copolymer of polyethylene oxide and polypropylene oxide. While both polypropylene oxide and polyethylene oxide are water soluble at low temperatures, polypropylene oxide becomes increasingly hydrophobic at higher temperatures. Therefore, the polymer will gel at temperatures and concentrations above a critical point [74].

Hydrogels were prepared for robocasting by utilizing this thermoreversible gelling behavior. It was important to develop a procedure that resulted in gels free of air bubbles and aggregates which would interfere with even extrusion. First, a stock solution of 25 wt.% Pluronic F127 was prepared by slowly adding the polymer to water with stirring in an ice bath. Once fully dissolved, the solution was transferred to the planetary ball mill for 1 min to fully homogenize. The hydrogel was left in an ice bath overnight to defoam. Next, powder was added to the solution while below the gel point of 18°C. This was done

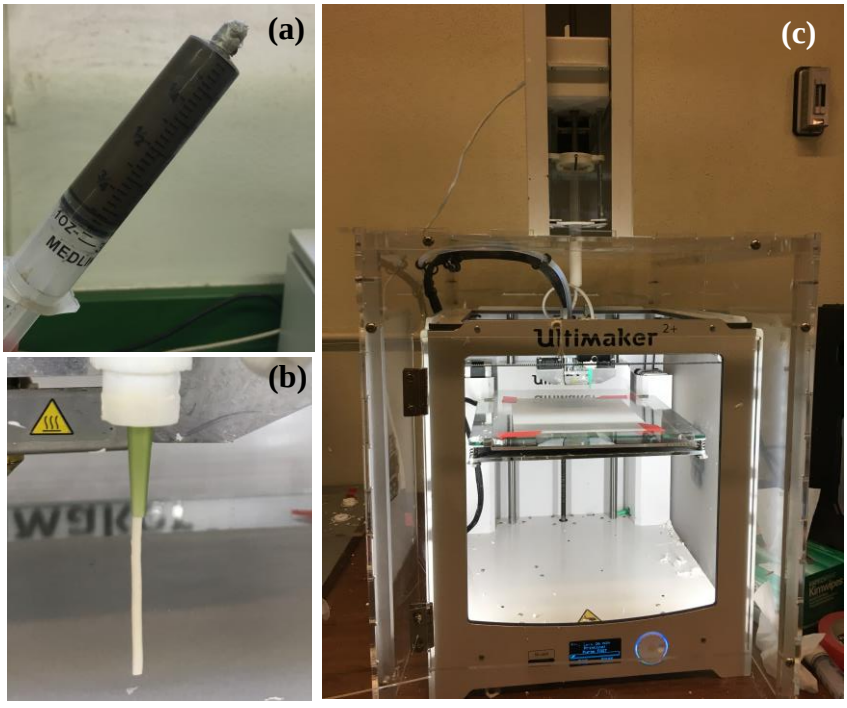

Figure 3.5. Images of the robocasting process: **(a)** syringe of basalt filled hydrogel, **(b)** even extrusion of hydrogel, and **(c)** setup of Ultimaker 2+/Discov3ry robocasting 3D printer.

stepwise, with mixing being carried out by planetary ball milling in 1 min intervals, with chilling in between. After all the powder was added, the mixture was returned to the ball mill for 3 min to homogenize and defoam. The hydrogels were stored at room temperature, then transferred to 10 mL syringes when ready for robocasting.

Robocasting of the mineral filled hydrogels was done in the LIAM lab on an Ultimaker 2+ FDM 3D printer equipped with Discov3ry paste extruder attachment, shown in Figure 3.5. The provided slicing software, Cura, was used to define printing parameters and toolpaths [75]. Printing parameters were optimized to create a visibly dense structure. Print speed and material flow were adjusted to give even extrusion and prevent the extrudate from being stretched during printing.

Samples were 3D printed using various nozzle sizes and printing parameters optimized based on the nozzle diameter. After printing, specimens were dried overnight at 100°C. Thermogravimetric analysis (TGA) of the dried samples was performed using a TA Instruments TGA55 in the materials characterization facilities. TGA measures the weight loss of a sample as a function of temperature, and so was used to determine a debinding temperature by finding the temperature at which all polymer was removed. TGA measurements were taken from 100 to 700°C at a heating rate of 10°C/min in air atmosphere.

CHAPTER 4: FUSED DEPOSITION MODELING OF ABS/MINERAL COMPOSITES

Fused deposition modeling (FDM) was used to prepare ABS composites filled with silica, basalt, or LRS powders. Both filled and unfilled ABS specimens were 3D printed for tensile testing to determine the effect each filler had on the mechanical properties of ABS. Filler loading was varied to determine the maximum filler that could be successfully incorporated into filaments for FDM. The effect of surface treatment and the differences in particle size distribution and morphology were also evaluated. The obtained results were compared and contrasted with available literature that focused on incorporation of 'pristine,' and relatively uniformly-sized filler powders. Details of this study are discussed in this chapter.

4.1 Mineral Powder Characterization

Before being introduced as filler in ABS filaments, the different filler systems were characterized using DLS and SEM to determine their size distribution and morphology, respectively. SEM images of the processed powders can be found in Figure 4.1. Average particle size and particle size distributions are listed in Table 4.1. The average particle size of the silica was 0.9 ± 0.3 μm with a relatively narrow particle size distribution. The silica particles were irregularly shaped but with an aspect ratio close to one. The ground basalt particles were also irregular with some acicular particles and had a smaller average particle size of 0.6 ± 0.3 μm. The particle size distribution for basalt was much broader than the silica powder, with smaller particles being observed to aggregate onto larger particles in the SEM images. After grinding, the LRS had a similar average particle size and size distribution as the basalt powder, with the average particle size being 0.7 ± 0.4 μm. However, the LRS was a mixture of irregular

platelets, and acicular particles. The broad particle size distribution of the basalt and LRS powders attributed to the processing method, with minerals of different hardness being fractured at varying rates.

Table 4.1: Characterization of Mineral Powder for Use in ABS Composites

Powder	Processing	Average Particle Size	Particle Size Distribution
Silica	as received	0.9 ± 0.3 µm	0.7 – 1.2 µm
Basalt	ground for 6 hours, filtered to <10 µm	0.6 ± 0.3 µm	0.3 – 5.7 µm
LRS	ground for 6 hours, filtered to <10 µm	0.7 ±0.4 µm	0.4 – 5.7 µm

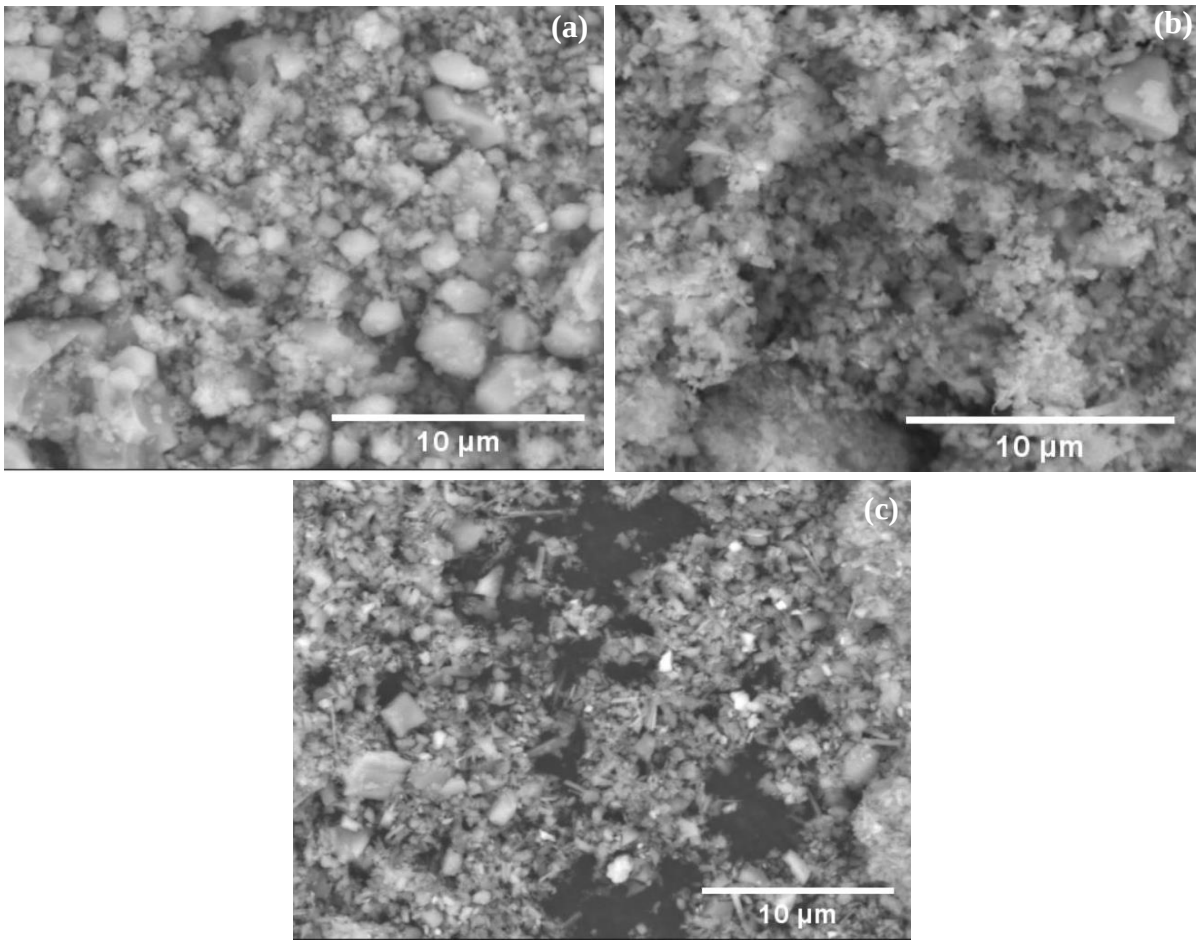

Figure 4.1. SEM images of **(a)** silica powder, **(b)** basalt powder, and **(c)** LRS powder. The basalt and LRS were ground to give the powdered sample.

4.2 Production and 3D Printing of ABS/Mineral Composite Filaments

To determine the maximum amount of filler loading possible using this experimental method, silica was added to ABS at concentrations of 1, 3, 5, and 7 wt.%. With loading up to 5 wt.%, smooth and homogeneous filaments were produced with the desired diameter of 1.75 ± 0.10 mm. However, as the loading increased to 7 wt.% silica, inhomogeneous filaments with visible agglomerates of silica were obtained. When surface treated silica (with silane or stearic acid) was introduced at concentrations of 5 and 7 wt.%, the results were similar; specifically, both silane treated and stearic acid treated silica powders were used to successfully extrude filaments with 5 wt.% filler.

Silane treatment yielded notably more brittle filaments, with filament breakage in the extruder gears occurring several times during the production of tensile test specimens. Alternatively, stearic acid acts as a lubricant and treatment of the silica produced more flexible filaments, although mixing of the filler at concentrations above 5 wt.% was still unsuccessful.

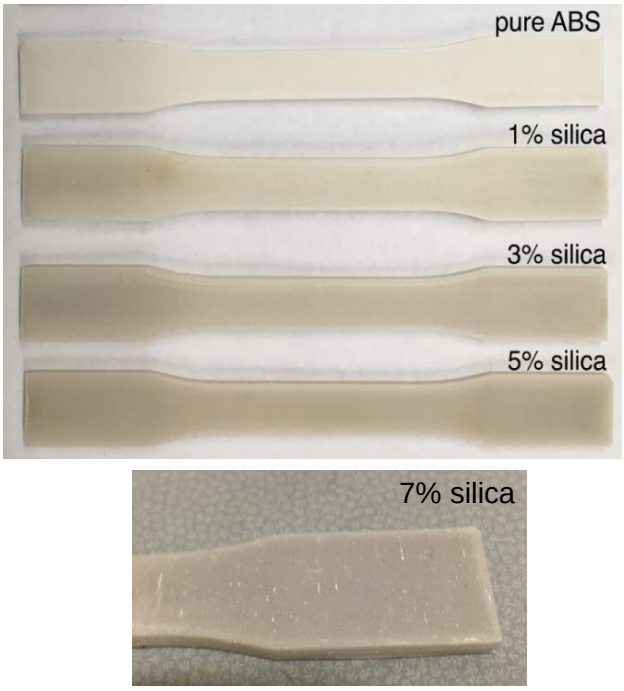

Figure 4.2. Tensile test specimens produced with increasing amounts of silica filler.

Keeping in mind the limits imposed on the filler fraction that could be incorporated, composite parts were 3D printed using 5 wt.% treated or untreated silica. It has to be noted that when attempting to use the composite filaments containing 7 wt.% silica, it became common for the nozzle to clog or the filament

to break in the extruder gears. Along with the difficulties in printing, silica aggregates were still visible in the printed part, as shown in Figure 4.2.

Due to the difficulty in 3D printing and visible inhomogeneity of the specimens containing 7 wt.% silica, they were not considered for further evaluation. Using the experimental methods described in this work, 5 wt.% was determined to be the maximum filler loading possible to successfully produce ABS composites. Given these results, filaments containing basalt or LRS powder were produced using 5 wt.% filler for comparison.

The filaments were analyzed by DSC to determine whether the addition of filler would alter the processing temperature needed for 3D printing the composite filaments. Heating through the T_g of a polymer enabled the polymer to relax from a glassy to rubbery state due to an increase in chain mobility. DSC curves shown in Figure 4.3 were used to determine the glass transition point (T_g) of the material, which is found as the middle of the sloped region seen in the

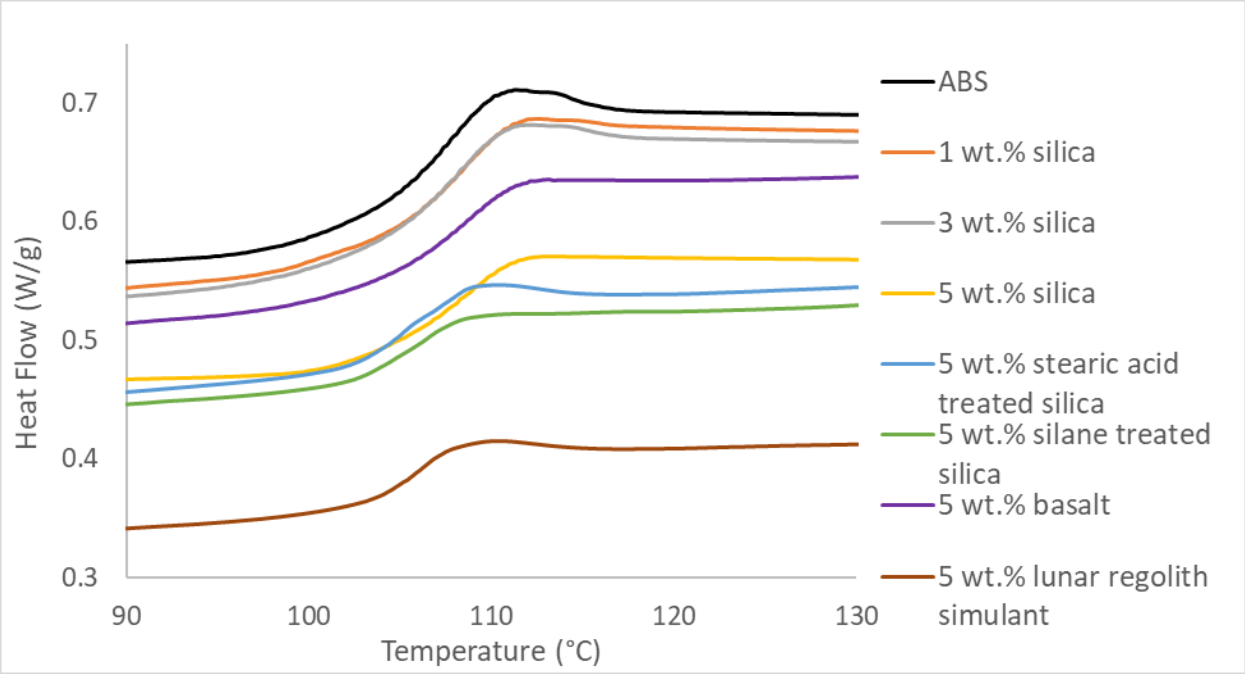

Figure 4.3. DSC curves of ABS and ABS composite filaments, showing negligible change in Tg with the addition of filler.

step-wise change in heat capacity of the polymer. Interactions between the matrix and filler can inhibit chain mobility and may lead to an increase in T_g [76]. Alternatively, particles that exert a repulsive force on the polymer may lead to a decrease in T_g.

Based on Figure 4.3, the ABS filaments were found to have a T_g of 107°C. All other filaments had a T_g between 106 and 109°C. Filaments produced with untreated filler were found to have a slightly higher T_g of 108-109°C, while the surface treated silica filaments had a T_g of 106°C. However, these very slight variations are within the expected range of T_g for pure ABS and inconclusive to the effect of the different fillers on chain mobility. No changes to the nozzle temperature were made based on these results.

The optimized printing parameters given in Table 4.2 were used to produce specimens that were visibly dense and within ± 0.5 mm of the desired dimensions. Filler decreased die swell when filament was extruded through the nozzle, so it was found necessary to increase the material flow rate slightly to compensate. A proper material flow rate was determined by printing a 20 mm cube and measuring the dimensions using digital calipers. The material flow was increased until the dimensions of the cube were 20 ± 0.10 mm. It was found that the material flow needed to be increased by 1% with each 1 wt.% filler added. For example, pure ABS was printed with a material extrusion multiplier of 1.00, while ABS containing 5 wt.% filler was printed with a material extrusion multiplier of 1.05.

A set of preliminary experiments were conducted to select the direction of infill to be used for fabricating tensile test specimens. Using infill solely in the direction of the applied tensile stress (i.e. 0° infill), yielded specimens with higher elastic modulus, ultimate tensile strength (UTS), and strain to failure when compared to those printed with alternating infill (i.e. 0°/90° infill). However, the samples printed at 0° infill tended to fail at a void existing where the

thin section of the specimen ended. Printing with alternating infill yielded denser specimens, which all failed within the thin section during tensile tests. The remainder of the ABS and ABS composite tensile test specimens were produced using these optimized printing parameters.

Table 4.2: Optimized Printing Parameters for ABS Composites

Nozzle size	0.6 mm
Extruder temperature	240°C
Bed temperature	115°C (first layer), 110°C
Layer height	0.35 mm (first layer), 0.20 mm
Print speed	25-30 mm/s
Infill	100% rectilinear, 0°/90°

4.3 Mechanical Properties of ABS Composites

Uniaxial tensile tests were conducted to evaluate the elastic modulus, ultimate tensile strength (UTS), and strain to failure of the various composites. These values were calculated in the instrument's software, according to the definitions given in ASTM D638 [77]. The elastic modulus the ratio of stress to strain in the region below the proportional limit, or below the point at which the stress-strain relationship deviates from Hooke's law. It is taken to be the tangent of the stress-strain curve at low stress values (within the elastic limit), or if calculated below the proportional limit:

$$E = \frac{\sigma}{\varepsilon} \tag{5}$$

where σ is stress and ε is strain. The ultimate tensile strength is the peak stress on the stress-strain curve, calculated as:

$$\text{UTS} = \frac{F_{max}}{A} = \frac{F_{max}}{T \times W} \tag{6}$$

where F_{max} is the maximum force sustained by the specimen, A is the original cross-sectional area, T is thickness, and W is width. Strain to failure reported in this work is the nominal strain, defined as

$$\varepsilon = \frac{\Delta l}{l_0} \tag{7}$$

where Δl is the change in grip separation and l_0 is the original grip separation.

Effect of untreated silica filler loading

Tensile tests were performed on ABS samples containing 0, 1, 3, or 5 wt.% silica to determine the effect of filler loading on the mechanical properties of 3D printed ABS. A representative stress-strain curve from each series of samples is given for comparison in Figure 4.4. The average mechanical properties from each set of specimens tested can be found in Table 4.3. The ABS samples had an average UTS of 35.4 MPa, which is lower than injection molded ABS, but typical of 3D printed samples due to voids and weak interlayer bonding intrinsic to the printing process [70], [78]. The average elastic modulus and strain to failure of ABS samples were 1512 MPa and 4.7%, respectively.

The most pronounced effect silica had on the mechanical properties of the 3D printed specimens was a decrease in the strain to failure. Even a small amount of silica embrittles the samples, with the strain to failure decreasing by 38% with the addition of 1 wt.% silica. Further increasing the silica loading did not have significant effect on the strain to failure. The silica composites had a slightly higher elastic modulus but also did not show a corresponding increase with increasing filler loading. At 1 wt.% silica did not affect the UTS of the printed parts, but

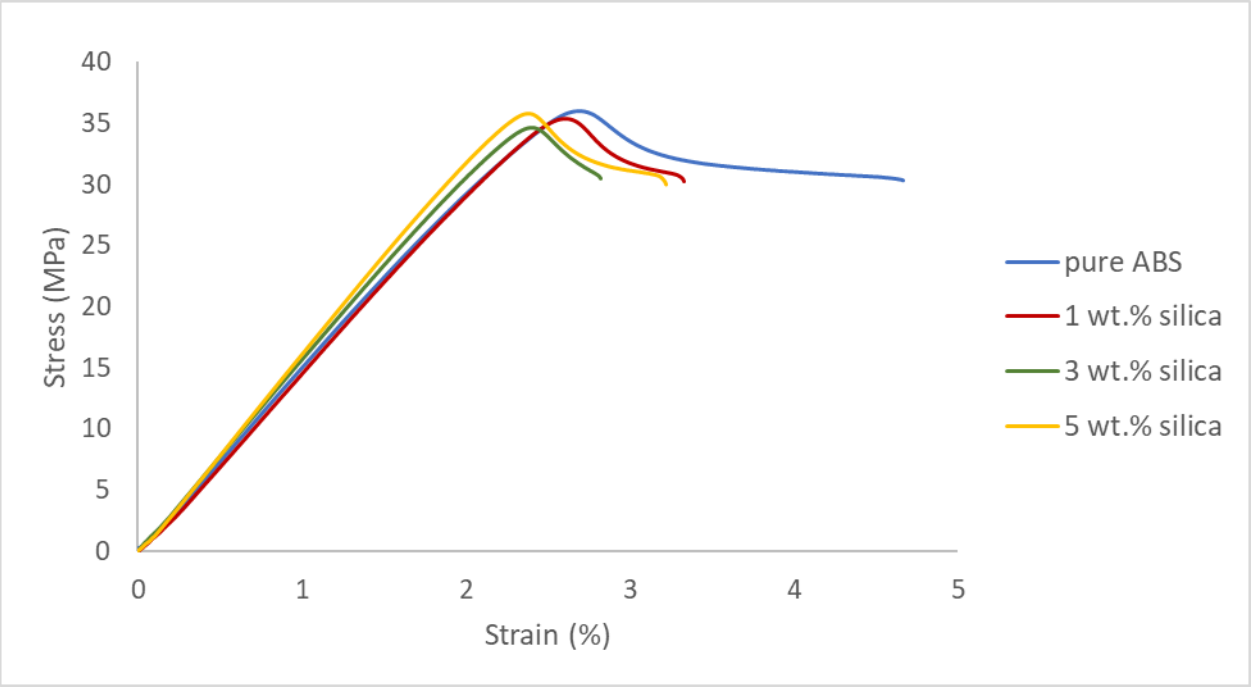

Figure 4.4. Stress-strain curves of ABS/silica composite 3D printed specimens with increasing filler loading.

Table 4.3: Average Mechanical Properties of ABS/Silica Composites

Silica Loading (wt.%)	Elastic Modulus (MPa)	UTS (MPa)	Strain to Failure (%)
0	1512 ± 34	35.4 ± 0.5	4.7 ± 0.6
1	1577 ± 38	35.4 ± 0.5	3.2 ± 0.4
3	1582 ± 23	34.7 ± 0.2	3.4 ± 0.3
5	1579 ± 97	34.0 ± 0.4	3.0 ± 0.2

the UTS tended to decrease with increasing filler loading. This decrease in strength was minimal with the UTS of the 5 wt.% silica composites being only 4% lower than pure ABS. Although increasing filler loading led to somewhat diminished mechanical properties overall, the quality of the printed parts was not compromised and increasing the filler loading led to a decrease in warpage during the printing process.

Fracture surfaces of the ABS/silica composites are shown in Figure 4.5. Voids are present due to incomplete filling between raster lines. In all samples, failure occurred primarily

along the interface of raster lines. The fracture surface of the pristine ABS samples (Figure 4.5a) shows deformation and fibrils characteristic to ductile failure in thermoplastics [79]. The V-shaped pattern of deformation is indicative of a tear fracture, in this case exposing the raster below. Macroscopically, the ABS sample showed significant stress whitening during the tensile test, usually assumed to indicate craze formation.

With increasing filler content, less deformation is seen on the fracture surface especially in the sample containing 5 wt.% silica, as shown in Figure 4.5d. For all concentrations, regions can be seen where silica particles were poorly dispersed or there are agglomerates with a size of

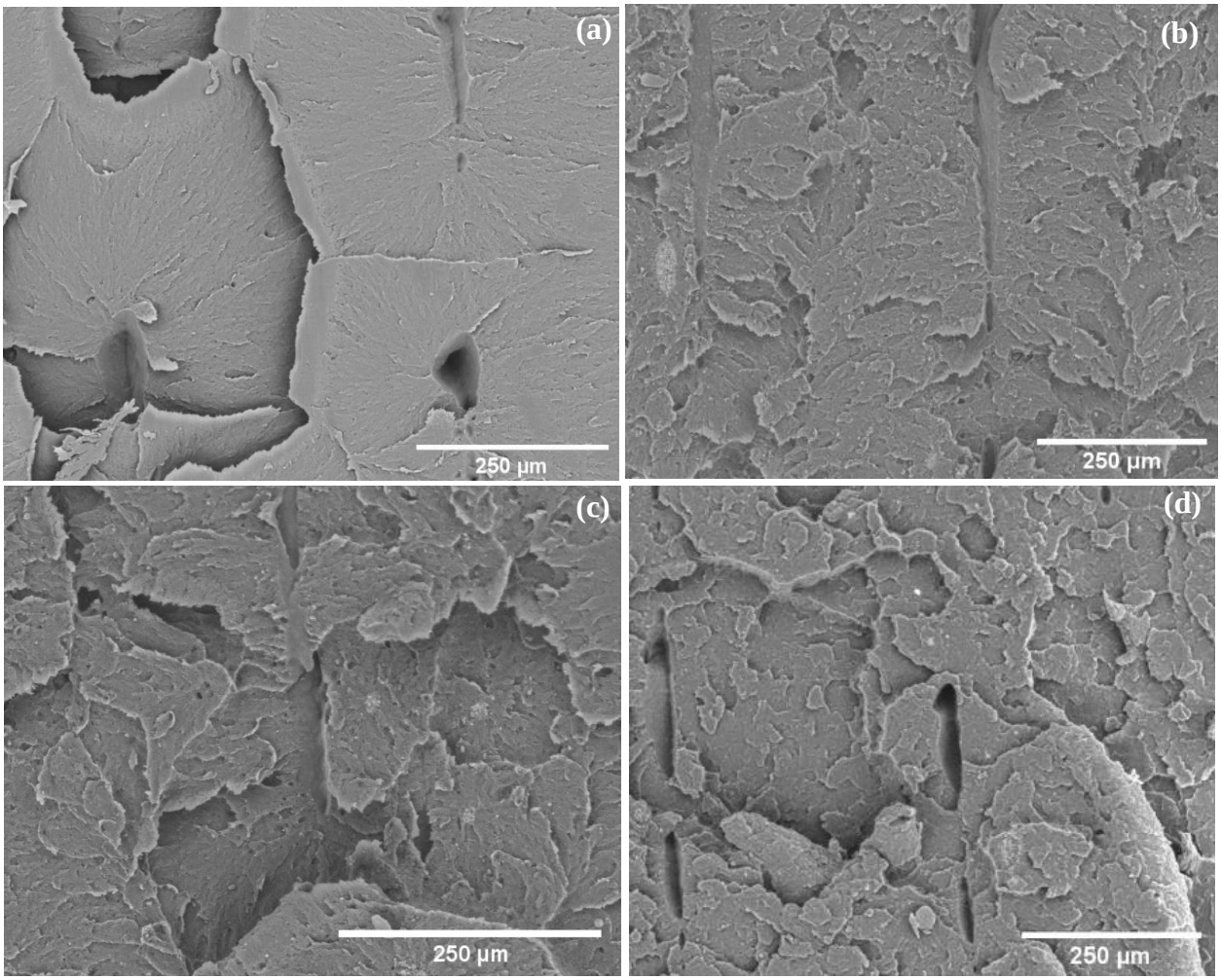

Figure 4.5. Fracture surfaces of 3D printed ABS with increasing silica loading: **(a)** 0 wt.%, **(b**) 1 wt.%, **(c**) 3 wt.%, and **(d)** 5 wt.%.

about 10 µm.

Effect of surface treatment of the filler

Treated silica was used to create composite parts at the maximum possible filler loading of 5 wt.% to determine whether interactions between the filler and polymer could be altered to increase the amount of filler added or improve upon the mechanical properties.

Surface treatments are performed to provide a coupling agent between hydrophobic inorganic fillers and hydrophilic polymers, providing better wetting between the two phases in the composite. However, surface treatment was not effective for increasing filler loading above 5 wt.% as agglomerates of silica particles were still present. Stress-strain curves comparing specimens prepared with untreated silica, silane treated silica, and stearic acid treated silica are given in Figure 4.6 and the average mechanical properties are in Table 4.4.

Silane coupling agents react with surface hydroxyl groups to bind to oxides and contain

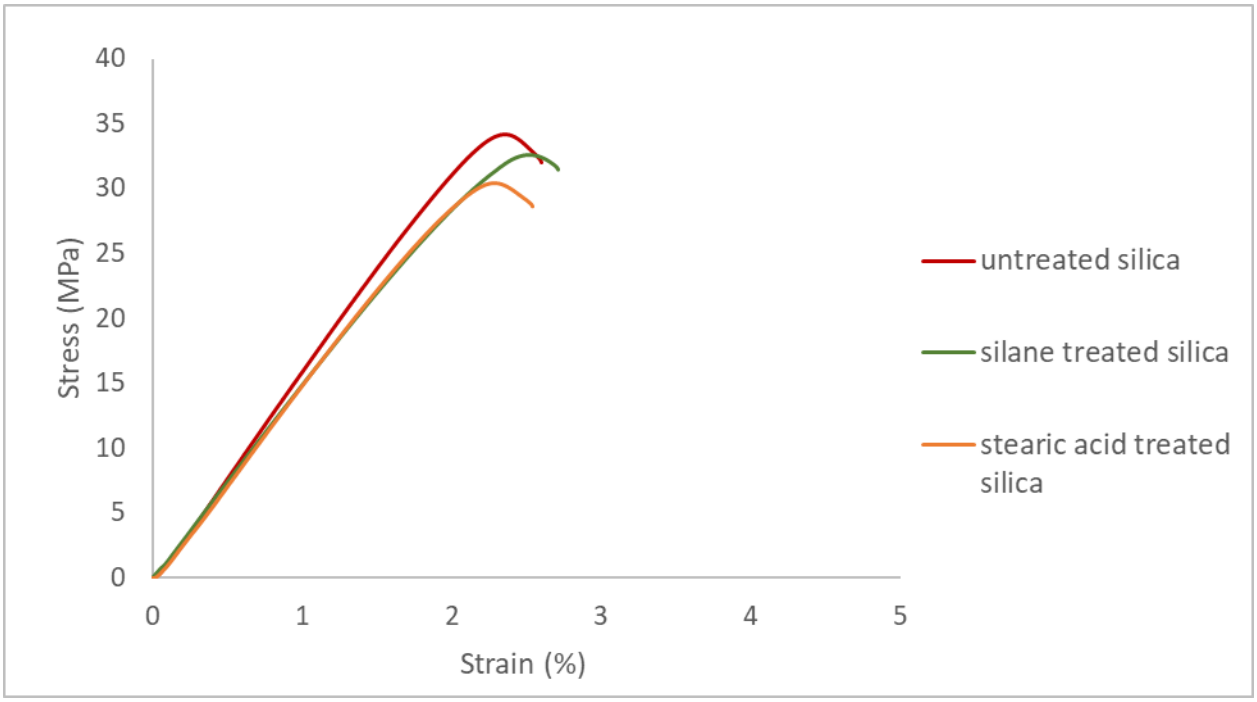

Figure 4.6. Stress-strain curves of 3D printed ABS/silica composites, comparing the effect of filler surface treatment with silane or stearic acid.

Table 4.4: Effect of Surface Treatment on Average Mechanical Properties of ABS/Silica Composites

Surface Treatment	Elastic Modulus (MPa)	UTS (MPa)	Strain to Failure (%)
none	1579 ± 97	34.0 ± 0.4	3.0 ± 0.2
silane	1555 ±32	34.0 ± 0.7	2.8 ± 0.2
stearic acid	1535 ± 71	31.6 ± 0.7	2.7 ± 0.1

an organofunctional group that bonds to the polymer [80]. Silane treatment of the silica did not affect the UTS of the composite parts. These composite filaments were especially brittle,

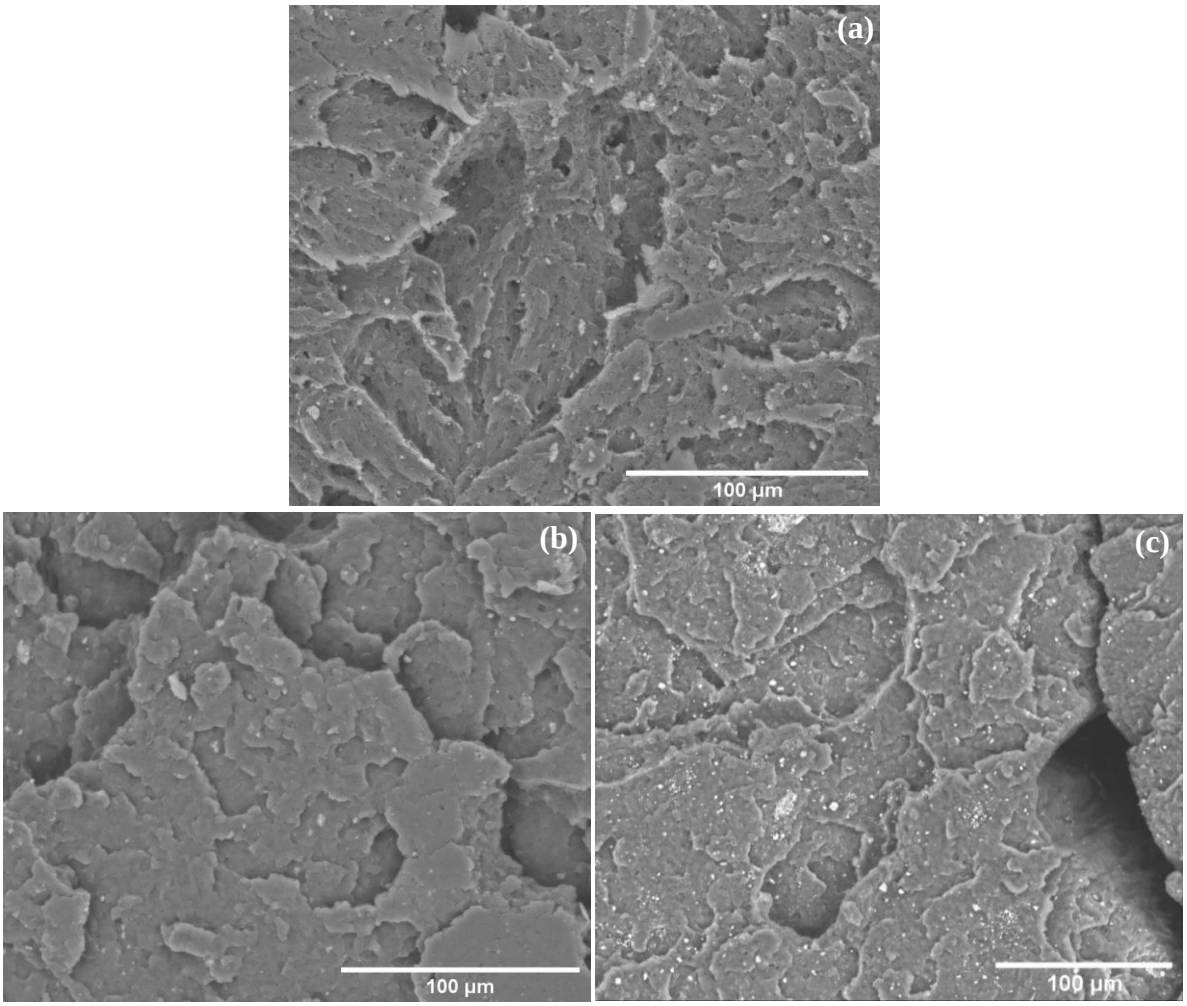

Figure 4.7. Fracture surfaces of 3D printed ABS/silica composites, with or without surface treatment: **(a)** untreated, **(b)** silane treated, and **(c)** stearic acid treated.

making them difficult to 3D print. The strain to failure of the 3D printed specimens was slightly lower than that of the specimens containing untreated silica. The elastic modulus was also slightly lower with silane treatment. As seen in a representative fracture surface shown in Figure 4.7b, silane treatment did provide better adhesion between the ABS and silica filler. This is evidenced by a lack of voids in the fracture surface as compared to the specimen containing untreated silica shown in Figure 4.7a, indicating poor wetting of the untreated silica particles by ABS. The fracture exhibits more brittle failure than that of the untreated silica specimen, showing less deformation and shorter fibrils. A relatively even dispersion of the silica particles was accomplished with silane treatment; however, agglomerates up to 10 μm are still visible.

Stearic acid is a fatty acid which is used to physically coat inorganic particles. It acts as a surfactant, increasing interfacial interaction between the polymer and filler particles [81]. Stearic acid treatment of silica particles led to a lowering of the UTS by 7% compared to composites prepared with untreated silica. The addition of stearic acid also slightly decreased the elastic modulus. The strain to failure of the 3D printed specimens was lower than both the specimens containing untreated silica and silane treated silica. Fracture surfaces, shown in Figure 4.7c, indicated that silica dispersion was poor using this surface treatment. Many areas of concentrated silica particles are visible along the fracture surface, as well as agglomerates of silica particles of a similar size to those in the other composites.

Comparison of mineral fillers

Based on the results from utilizing silica filler in ABS, basalt and LRS composites were prepared at a concentration of 5 wt.%. Tensile test specimens as shown in Figure 4.8, demonstrated that the basalt and LRS based mineral powders could be used to create composites at this filler loading without sacrificing print quality. Representative stress-strain curves of

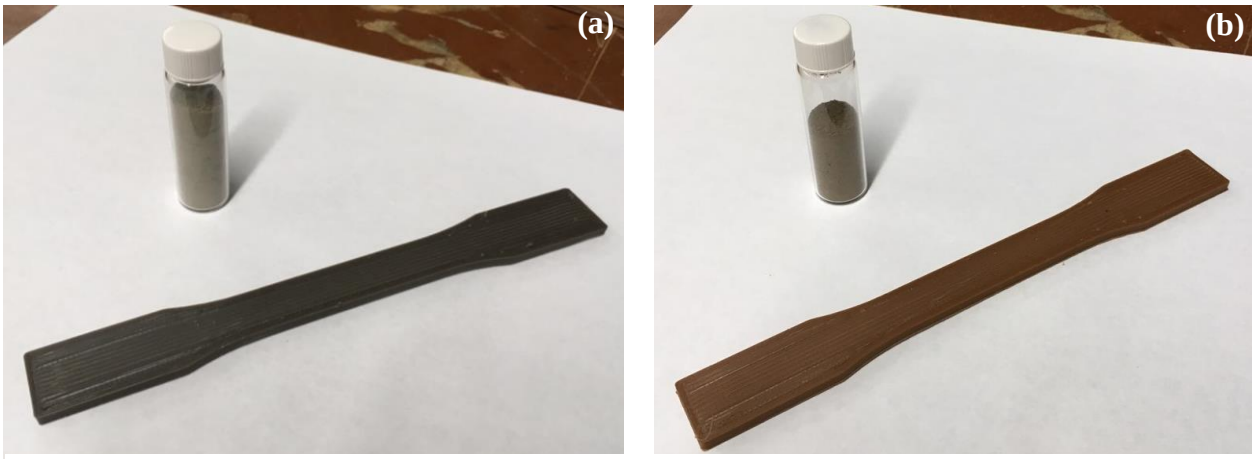

Figure 4.8. **(a)** Basalt and **(b)** LRS powders used as filler in ABS filaments and resulting 3D printed composite tensile test specimens.

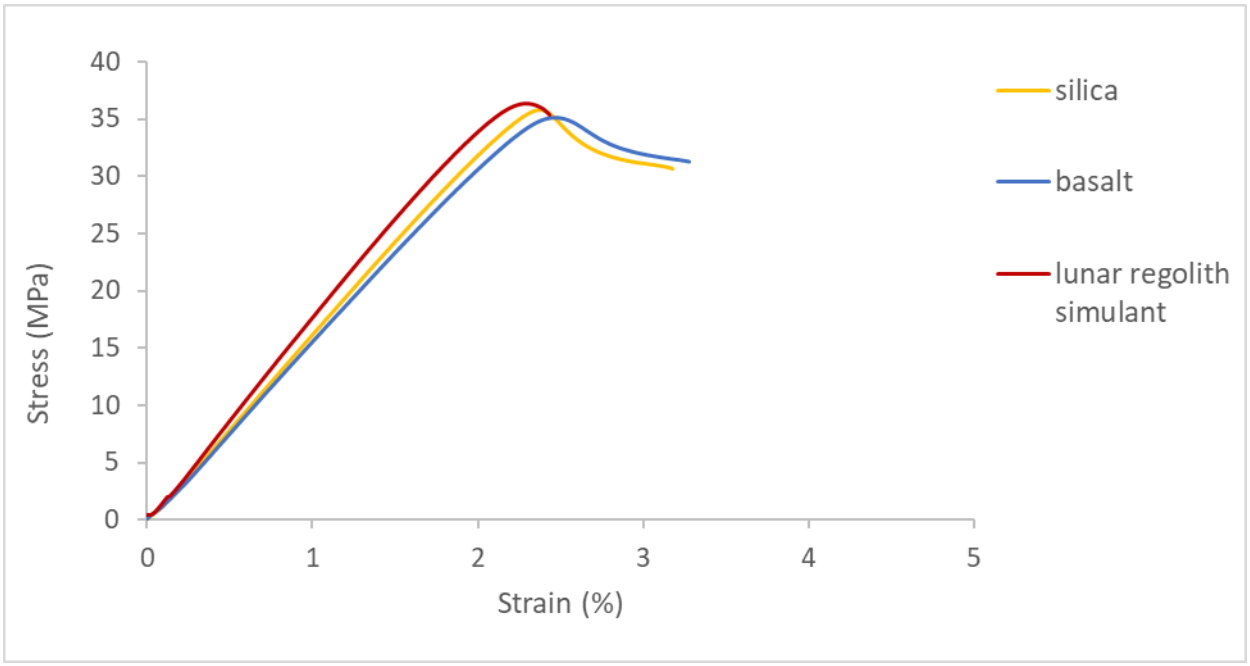

Figure 4.9. Stress-strain curves of 3D printed ABS composites containing 5 wt.% silica, basalt, or LRS.

ABS/silica, basalt, and LRS composite specimens are given in Figure 4.9 and the average mechanical properties from each set of specimens can be found in Table 4.5.

Basalt composites had similar mechanical properties compared to silica composites despite the differences in particle size distribution. The UTS was slightly decreased compared to ABS specimens. These composites showed a 6% increase in elastic modulus over pure ABS,

Table 4.5: Average Mechanical Properties of ABS/Mineral Composites

Filler (5 wt.%)	Elastic Modulus (MPa)	UTS (MPa)	Strain to Failure (%)
silica	1579 ± 97	34.0 ± 0.4	3.0 ± 0.2
basalt	1603 ± 26	34.3 ± 0.8	2.9 ± 0.3
LRS	1707 ± 91	32.0 ± 2.5	2.5 ± 0.2

which is slightly higher than that of the ABS/silica composites. The strain to failure was also similar to the ABS/silica composites containing 5 wt.% filler, with the samples failing at 2.9% strain. As seen in Figure 4.10a, the ABS/basalt composites also show regions in the fracture surface of poorly dispersed basalt particles and agglomerates with a size of ~10 μm.

LRS produced composites with the highest elastic modulus, lowest UTS, and lowest strain to failure compared to those filled with untreated silica or basalt. A decrease in strain to failure accompanied by an increase in elastic modulus is commonly observed in polymer/particulate composites, however the UTS of the composites is usually also higher than that of the polymer [28]. The elastic modulus of the ABS/LRS composites showed a 12%

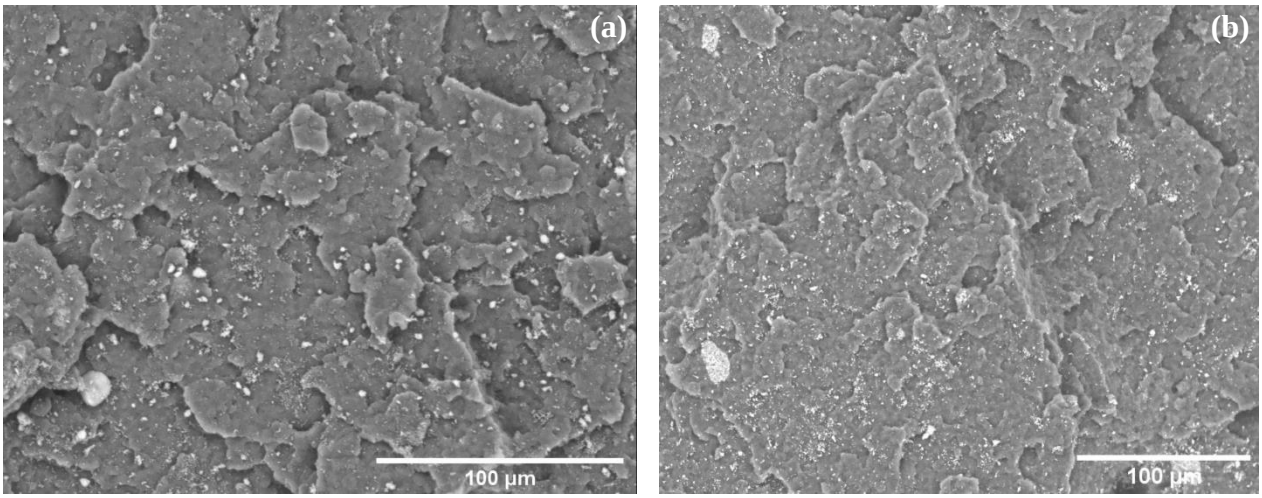

Figure 4.10. Fracture surfaces of 3D printed ABS/mineral composites containing 5 wt.% **(a)** basalt or **(b)** LRS.

increase over ABS specimens, providing about twice the reinforcing effect compared to the other ABS/mineral composites. The average UTS was 10% lower than ABS, while the strain to failure was decreased by 61%. The fracture surfaces, with an example being shown in Figure 4.10b, exhibited poor dispersion of the filler. The LRS dispersed significantly more poorly than the other silica or basalt powder, with many areas of high powder concentration and large agglomerates being observed.

4.4 Discussion

The addition of filler had the effect of slightly lowering the UTS of the composites in all cases, with the LRS giving the most dramatic reduction. Silica has previously been shown to strengthen [82] and toughen [83] ABS when composites were prepared by *in situ* sol-gel processing. However, the strength of the composites prepared in this work by melt processing in a single screw extruder is limited by the addition of silica filler. This indicates that the adopted processing method is insufficient to properly disperse the silica particles and create an intimate mixture between the two phases. The trend of decreasing tensile strength with increase in silica loading is consistent with this theory, as low concentrations of particles would be expected to disperse more readily. Fracture surfaces showed that both silane and stearic acid treatment improved wetting of the silica particles by ABS. However, silane treatment improved the dispersion of silica particles while dispersion was worsened by treatment with stearic acid. Stearic acid treatment yielded the lowest UTS of all the composites, suggesting that poor dispersion of filler is the main cause of the decrease in tensile strength with the addition of mineral fillers. Effective load transfer cannot be accomplished without even dispersion of filler in the ABS matrix.

As a rigid phase is being introduced, it would be expected that the addition of filler would increase the modulus of the composites according to the rule of mixtures. Although the addition of silica initially provided a reinforcing effect, the elastic modulus did not prove to be impacted by silica loading over the range studied in this work. Surface treatment of the silica particles led to a slight lowering of the elastic modulus, as compared to untreated silica. However, surface treatment should enhance polymer/filler adhesion and it was expected that this would lead to an increase in elastic modulus. This contradictory observation needs further analysis which is beyond the scope of this work. It is likely that filler loading is too low to have a significant effect on the elastic modulus, especially because the poor dispersion of the filler reduced the surface area of the filler contacting the ABS matrix. These results are consistent with other research utilizing low aspect ratio fillers in ABS at loading of 5 wt.% [58], [84]. Both basalt and the LRS increased the stiffness as compared to silica, with the LRS having the most pronounced effect. This effect is likely due to the acicular morphology of the particles. There has already been extensive research showing that high aspect ratio particles have a stronger reinforcing effect [85].

Strain at failure is often lowered with the addition of filler, as filler can act as crack initiation sites and reduce the extensibility of the polymer phase [85]. The composite filaments could no longer be printed when the filler content was above 5 wt.%. Due to aggregation of powder in the nozzle and the brittleness of the resulting filaments, clogs and filament breakage in the extruder became common at higher loadings. The use of reinforcing filler in FDM is limited compared to traditional manufacturing methods, with filler loading generally being limited to 10 wt.% or less [42], [43], [57], [58]. The mechanical properties of parts produced by FDM are consistently lower than injection molded parts due to weak interlayer bonding, interlayer voids,

and residual stresses caused by shrinkage [78]. The addition of defects from weak adhesion with inorganic particles and the present of large particles or aggregates may be much more detrimental in a part produced using FDM than an injection molded part.

Improving dispersion of the mineral fillers used in this work could potentially improve the mechanical properties of ABS composites. The Filabot single screw extruder had the benefit of being portable and low cost, but it does not provide the high shear force that a twin screw extruder can provide to effectively break up agglomerates and disperse the particles. Other works have used solvent based methods to maximize filler loading; however the advantage of using *in situ* resources provided by mineral filler would be counteracted by the need for solvent and a proper reclamation system [53], [55].

Although improvements to the mechanical properties of ABS were limited, the composites produced in this work could be applied in place of pure ABS in many situations if parts are designed for these known mechanical properties. The UTS of the composites was at most 10% lower than pure ABS, which is still within the range of strength needed in many applications. With up to 5 wt.% of filler loading, the visual appearance and quality of the printed parts was not affected by filler except for the color change. As seen in Figure 4.11, the composite filaments can be used for the fabrication of complex and useful parts. In fact, the use of filler decreased

Figure 4.11. Nuts and bolts 3D printed from ABS containing 5 wt.% silica (left), basalt (center), or LRS (right).

shrinkage and warping during the printing process. Thus, up to 5 wt.% of silica, basalt, or lunar regolith fillers may be utilized in ABS fillers without significantly affecting the FDM process.

4.5 Summary

- The maximum filler loading accomplished was 5 wt.% for all ABS/mineral composites, above which poor mixing led to nozzle clogging and filament breakage during the FDM process.
- ABS/silica composites showed an increase in elastic modulus, decrease in UTS, and decrease in strain to failure, although there were no clear trends between these properties and filler loading.
- ABS/basalt and ABS/LRS composites displayed an increase in elastic modulus compared to ABS/silica composites.
- Mechanical properties of all ABS/mineral composites are likely limited by poor dispersion of particles, indicating a change in processing method may yield improvements.

CHAPTER 5: ROBOCASTING OF MINERAL FILLED HYDROGELS

Robocasting was explored as a method to maximize the use of *in situ* resources in additive manufacturing by formulating hydrogels with a small amount of Pluronic F127 binder to create ceramic structures composed of native minerals. To this end, the concentration of silica, basalt, or LRS powder in a hydrogel carrier was varied to create inks of suitable viscosity and strength for the robocasting process. This chapter provides experimental results of this study and discusses the feasibility of creating structural ceramics using the developed method.

5.1 Processing and Characterization of Minerals

Silica, basalt, and LRS powders were prepared with the minimal processing required for use in the robocasting process. The results of this processing are given in Table 5.1. The average particle size of the silica powder was 0.9 ± 0.3 μm and the particle size distribution was 0.7-1.2 μm, as determined by DLS measurements. Basalt was also previously characterized by DLS and found to have an average particle size of 0.7 ± 0.3 μm and a particle size distribution of 0.3-5.7 μm. The size distribution of the LRS was classified using 180 and 45 μm sieves and a 10 μm filter, with the results as shown in Figure 5.1a. Particles smaller than 180 μm were used in the robocasting process, to ensure that large particles would not aggregate and form clogs in the nozzle. As seen in the SEM image given in Figure 5.1b, the LRS contains many large particles with high aspect ratio. Sieving should be carried out using a mesh with a size much smaller than the nozzle diameter to prevent acicular particles with a length near the diameter of the nozzle passing through. The average particle size was in the range of 45-180 μm.

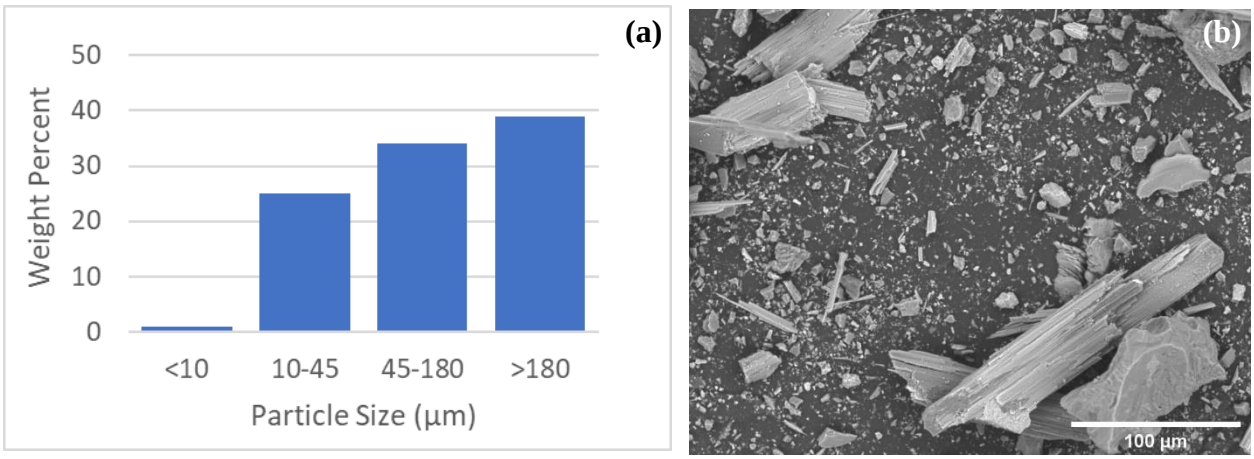

Figure 5.1. (a) Particle size distribution and **(b)** SEM image of LRS, as received.

Table 5.1: Characterization of Mineral Powders for Use in Robocasting

Mineral	Processing	Average Particle Size	Particle Size Distribution
Silica	as received	0.9 ± 0.3 µm	0.7-1.2 µm
Basalt	ground for 6 hours, sieved to <10 µm	0.6 ± 0.3 µm	0.3-5.7 µm
LRS	sieved to <180 µm	45-180 µm	<10-180 µm

5.2 Preliminary Investigation of Mineral-Filled Hydrogels as Robocasting Feedstock

To determine the concentration of minerals that could be used to create a suitable robocasting ink, Pluronic F127 hydrogels were prepared containing 30, 35, or 40 vol.% mineral filler. As a preliminary investigation, these hydrogels were extruded by hand through a 0.84 mm nozzle attached to a 10 mL syringe. This qualitatively provided information on the viscosity of the hydrogels and the pressure required to extrude them. Furthermore, it could be tested whether the strength of the hydrogel was high enough to support subsequent layers and avoid slumping. The drying behavior showed whether the solid loading was high enough to avoid cracking due to

excessive shrinkage. The results of this brief experiment are described in Table 5.2 below, with images of the dried lattice structures given in Figure 5.2. Structures were successfully formed from hydrogels containing 35 or 40 vol.% silica, 30 or 35 vol.% basalt, and 30 or 35 vol.% LRS. Given these results, the formulations given above were used as robocasting feedstock.

Table 5.2: Syringe Extrusion of Hydrogels with Varying Concentrations of Mineral Filler

Mineral	Concentration (vol. %)	Results
silica	30	slumping, cracking during drying step
	35	adequate strength and viscosity
	40	adequate strength and viscosity
basalt	30	adequate strength and viscosity
	35	adequate strength and viscosity
	40	highly viscous, difficult to extrude
LRS	30	adequate strength and viscosity
	35	adequate strength and viscosity
	40	highly viscous, difficult to extrude

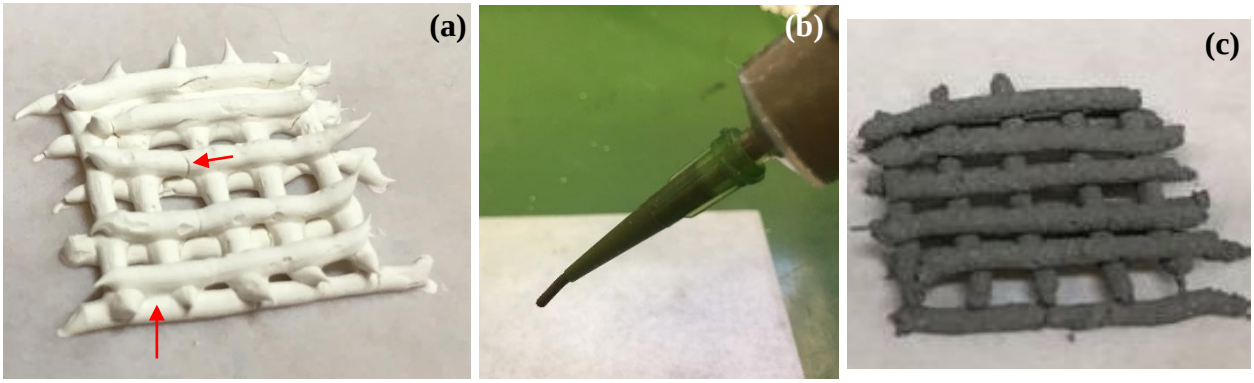

Figure 5.2. Results of syringe extrusion of mineral filled hydrogels, showing **(a)** cracking and slumping of dried structure extruded from 30 vol. % silica hydrogel, **(b)** high viscosity of 40 vol. % LRS hydrogel preventing flow, and **(c)** dried structure extruded from 35 vol. % basalt hydrogel maintaining desired shape.

5.3 Robocasting of Mineral-Filled Hydrogels

The hydrogels discussed previously were tested as robocasting feedstock. Initial trials determined that hydrogels on the higher end of filler loading (40 vol.% silica, 35 vol.% basalt, and 35 vol.% LRS) were not suitable for the robocasting system used in this work. The high pressures required to extrude these hydrogels led to uneven extrusion and failure at the luer locks connecting the polyethylene tubing to the syringe. The formulations with lower filler loading were successfully used, extruding smooth filaments with no visible aggregates or air gaps like those shown in Figure 5.3. Different nozzle sizes were also tested, with the hydrogels being successfully used with 0.61 mm, 0.84 mm, 1.19 mm, and 1.54 mm nozzles. The composition by of the hydrogels used throughout the remainder of this work are those given in Table 5.3.

Table 5.3: Composition of Mineral Filled Hydrogel Robocasting Formulations

	Mineral	**Pluronic F127**	**Water**
Silica	57 wt.% (35 vol.%)	11 wt.%	32 wt.%
Basalt	52 wt.% (30 vol.%)	12 wt.%	36 wt.%
LRS	57 wt.% (30 vol.%)	11 wt.%	32 wt.%

A brief experiment was also conducted to measure the flow rate of each material through the nozzle. Rueschhoff et al. previously used volumetric flow rate to determine the shear rate during the extrusion process, through the following formula:

$$\gamma = \frac{4Q}{\pi r^3} \tag{8}$$

where γ is shear rate, Q is volumetric flow rate, and r is the nozzle radius. The volumetric flow rate was determined by extruding hydrogels through a 1.19 mm nozzle for a set length of time and weighing several samples of extrudate. The mass flow rate was then converted to volumetric

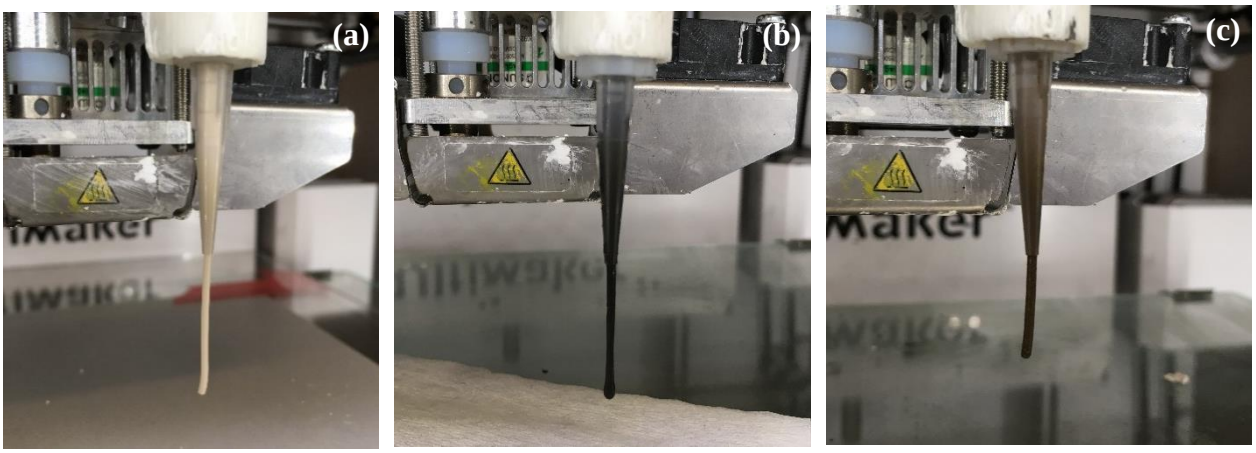

Figure 5.3. Extrusion through 1.19 mm nozzle of hydrogels containing **(a)** 35 vol.% silica, **(b)** 30 vol.% basalt, or **(c)** 30 vol.% LRS.

flow rate through the previously determined densities of the hydrogels, which were 1.64 g/mL, 1.59 g/mL, and 1.77 g/mL for the silica, basalt, and LRS formulations, respectively. Through this method it was determined that the 35 vol.% silica hydrogel had a volumetric flow rate of 1.1 mm^3/s, with the shear rate of extrusion being 6.5 s^{-1}. The hydrogel containing 30 vol.% basalt had a higher volumetric flow rate of 1.2 mm^3/s with a shear rate of 7.0 s^{-1}, while the 30 vol.% lunar regolith sample displayed a lower volumetric flow rate of 0.9 mm^3/s and a shear rate of 5.7 s^{-1}. These values were very similar despite the variations in the filler properties and it was found experimentally that the same printing parameters could be applied to the different hydrogels successfully.

Controllable variables in the robocasting process include the layer thickness, line width, flow rate, and print speed. Through trial and error, optimal printing parameters were found for a nozzle size of 0.84 mm, which provided a balance between resolution and speed. Layer thickness was chosen so that the nozzle did not drag through the previous layer and good contact between layers was achieved. The line width was adjusted for shape retention of the filament and maximum filling. The flow rate and print speed had to be adjusted to provide smooth extrudate without gaps or stretching caused by insufficient material deposition or compression

caused by too much material being deposited. The optimized printing parameters found in Table 5.4 were used to fabricate structures.

Table 5.4: Optimized Printing Parameters for Robocasting Mineral Filled Hydrogels

Nozzle size	0.84 mm
Layer thickness	0.84 mm
Line width	0.84 mm
Flow rate	40%
Print speed	5 mm/s

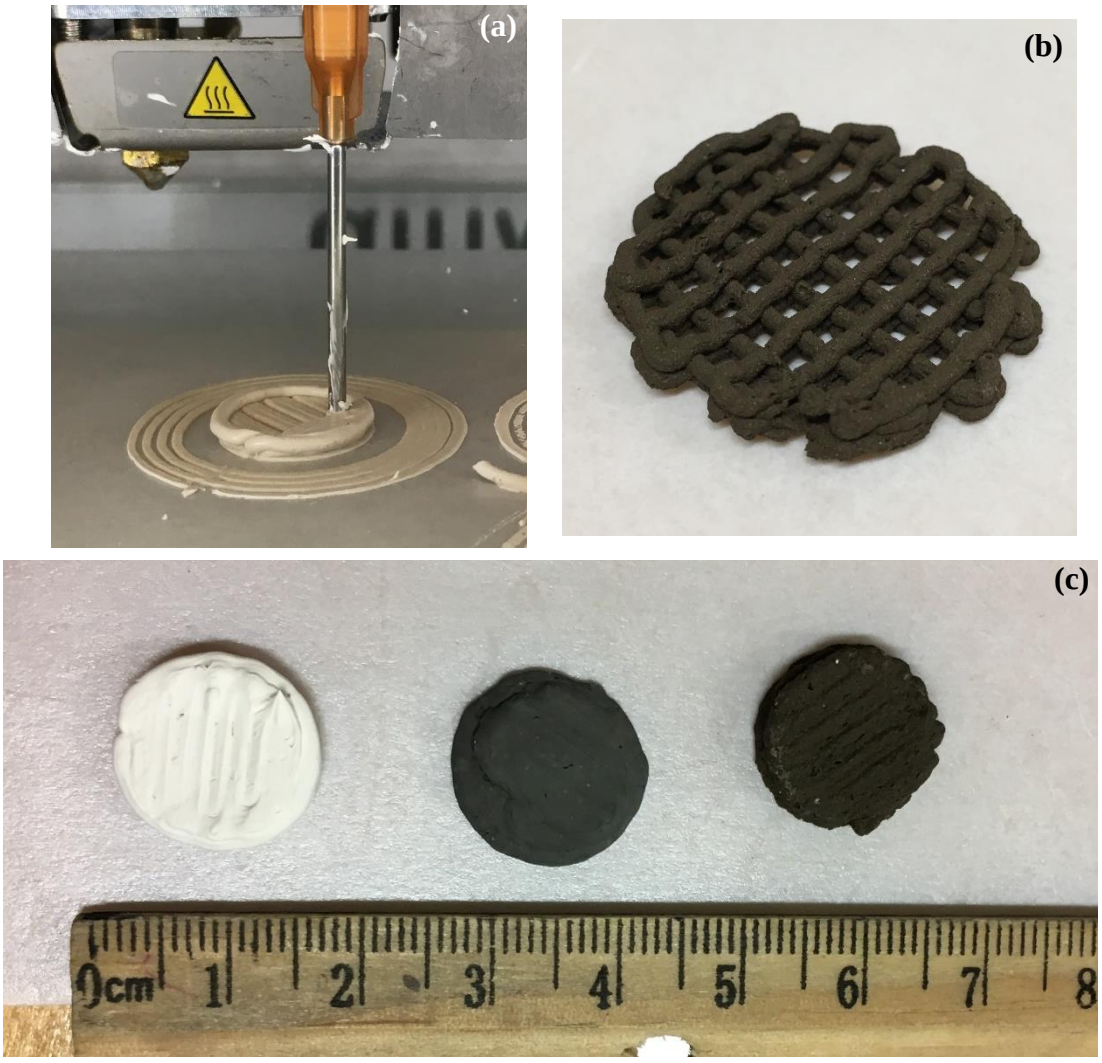

Figure 5.4. (a) Robocasting of silica filled hydrogel, **(b)** 3D printed green body lattice structure, and **(c)** 3D printed green bodies composed of silica (left), basalt (center), or LRS (right).

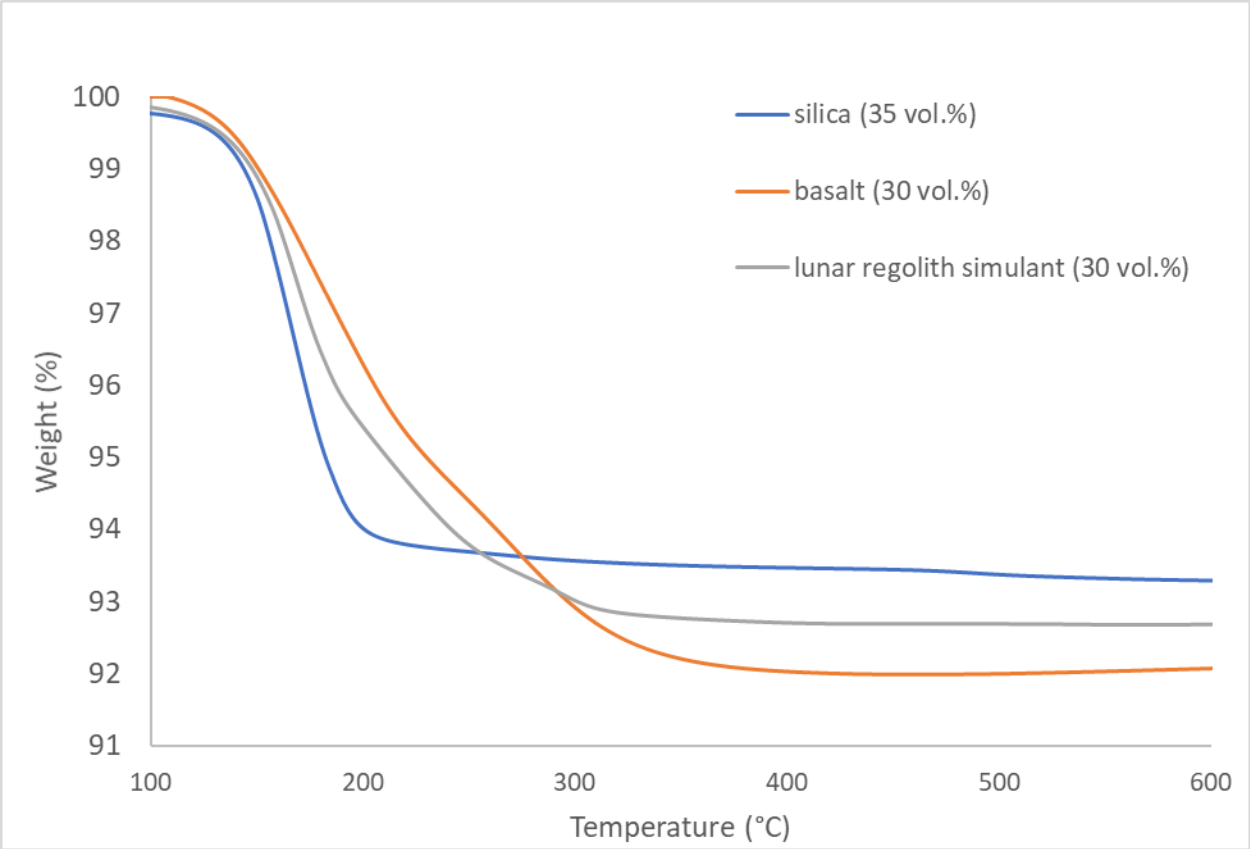

Figure 5.5. TGA curves of hydrogel filaments after drying to remove water. Data confirms that binder was fully removed at 600°C.

Figure 5.6. Silica, basalt, and LRS hydrogel filaments before (top) and after (bottom) drying and sintering steps.

TGA analysis of extruded filaments was carried out to determine the temperature needed to remove the polymer binder phase. The results, given in Figure 5.5, showed that binder was completely removed once

a temperature of 600°C was reached. Oxidation of the basalt and lunar regolith simulant occurred in this temperature range, as evidenced by an increase in the sample's weight during TGA analysis and a color change from grey to light brown of the basalt sample. Based on these results, filament samples were heated in a tube furnace in air atmosphere to 600°C at a rate of 10°C/min. The samples were held at 600°C for 1 hour to remove binder then heated further to 1000°C to sinter the powder particles. While future work will focus on determining optimal sintering temperature and duration that would lead to densification of 3D printed structures, current work has shown that solid filaments can be fabricated without visible defects from the debinding process, as can be seen in Figure 5.6.

5.4 Discussion

Despite major differences in particles size, particle size distribution, and morphology, the silica, basalt, and LRS powders could be 3D printed at concentrations of 30-35 vol.% using the robocasting process with Pluronic F127 hydrogel acting as a carrier. The volume fraction of solids will affect the extrusion behavior of pastes and determine the maximum concentration of solid loading possible. Particle packing behavior has been shown to alter the volume fraction of powder that can be added to form a printable paste, with bimodal particle size distribution allowing for better packing and increased solids loading [62], [73]. The maximum volume fraction accomplished in this work was using silica powder, which had the narrowest particle size distribution. The irregular morphology of the basalt and LRS powders likely leads to a less dense packing structure, with angular and elongated particles preventing smaller particles from filling empty spaces. Particle loading could be increased by refining powder processing methods to produce more regularly shaped particles with a broad particle size distribution. Powder

loading of 30-35 vol.% is comparable to previous work using Pluronic F127 for robocasting of ceramics [62], [64], [86]. Feilden et al. demonstrated the fabrication of 95% and 97% dense SiC and Al_2O_3 structures, respectively, through sintering of green bodies prepared using hydrogel inks [62].

The particle size did not influence the extrusion behavior, as basalt and LRS hydrogels were 3D printed at the same volume loading. The 3D printed structures composed of LRS did have a noticeably rougher surface, however. Utilizing particles with sizes up to hundreds of microns eliminates the need for grinding, which is the most time-consuming and energy intensive step in feedstock preparation. This method could be readily applied in remote environments where loose sand, regolith, or soil is present. Depending on the application, nozzle size can be varied with smaller nozzle providing better resolution and larger nozzles decreasing printing time and potentially accommodating larger particle sizes.

Structures were successfully fabricated that contained 52-57 wt.% mineral powders. The hydrogel is composed of 75 wt.% water, which could be reclaimed during the drying step. Only 10 wt.% of the feedstock is composed of polymer which is lost when sintering specimens. This provides a pathway for producing complex multi-component ceramic structures using 90 wt.% *in situ* resources.

5.5 Summary

- Pluronic F127 hydrogels filled with 30-35 vol.% mineral powder were found to have suitable particle loading to form an easily extrudable paste for robocasting.
- Basalt and LRS formed higher viscosity pastes, due to low packing densities of irregularly shaped particles.

- Structures were 3D printed and dried to prepare green bodies with ~90 wt.% silica, basalt, or LRS for sintering.

CHAPTER 6: CONCLUSIONS

This work explored two methods of utilizing *in situ* mineral resources in additive manufacturing, each with their own applications. The conclusions drawn from this work can be used to guide *in situ* resource utilization by expeditionary forces on Earth and in future Lunar exploration. The limitations of this work and recommendations for future work in this research area will also be given below.

Earth-abundant minerals and LRS were utilized as filler in ABS to fabricate structures by FDM. The addition of filler provided minimal improvements to the stiffness of 3D printed parts, with an increase in the elastic modulus up to 12% being seen in ABS/LRS composites. All the ABS/mineral composites showed a reduction in strain to failure. The UTS of the ABS/mineral composites was also slightly lower than pure ABS, with the maximum decrease in UTS being 10% in the ABS/LRS composite. Tensile testing and analysis of fracture surfaces suggest that the mechanical properties of the 3D printed samples are limited by the filament processing method. The mineral fillers are prone to aggregation and the use of a single screw extruder was found to be insufficient to properly disperse them in the ABS matrix. Surface treatment of silica by silane or stearic acid had little impact on dispersion and mechanical properties.

Despite these limitations on the mechanical properties, up to 5 wt.% of filler could be introduced without making significant changes to the processes of filament production and FDM. 3D printed ABS/mineral composites can be prepared in place of pure ABS without modifications to existing equipment being used in remote environments. The only additional equipment needed is a planetary ball mill or sieves to collect micron sized mineral powders. Mineral composites prepared using the method given in this work provide a 5% decrease in the weight of

polymer that needs to be carried in, providing a small savings on transportation and material costs. This impact could potentially be greatly increased by combining mineral fillers with recycled ABS collected from defunct parts. Recycling ABS has been shown to decrease the elastic modulus of 3D printed parts [10], so the addition of mineral fillers could potentially counteract this effect. Native mineral resources are an effective *in situ* resource to extend the polymer matrix and can be used in their unrefined state to create ABS composites at low filler loading. The composites were used in the FDM process to fabricate complex parts on demand.

To decrease the amount of polymer required to produce structures, *in situ* minerals may be used as the main source of feedstock and combined with a polymer binder for the robocasting process. This yields multicomponent structural ceramics after sintering. In this work, hydrogel feedstock was created containing 52-57 wt.% mineral powders and ~10 wt.% organic binder, with the remainder being water. Assuming a water source has already been identified in remote environments, ceramics may be constructed with a majority of *in situ* resources. Particle size was found to have little effect on the filler loading achieved in the hydrogels. Maximum filler loading was the same by volume for ground basalt powder with particle size ranging from 0.3-5.7 μm and sieved LRS with particle size between <10 μm to 180 μm. Therefore, regolith can be sieved to removed very coarse particles and then used without further processing to rapidly produce robocasting feedstock.

The volume loading of minerals used in Pluronic F127 hydrogels in this work is comparable to previous robocasting works in which dense ceramic structures were fabricated [62], [64], [86]. It is also comparable to work by Jakus et al. to produce LRS composites in a solvent based robocasting method [23], which was later shown by Taylor et al. to produce sintered lattice structures with strengths similar to commercial ceramic foams [24]. The volume

loading could be increased by altering powder processing techniques to achieve more regularly shaped particles and a higher powder packing density. Further investigation should be carried out to determine the sintering behavior of the green bodies produced in this work and resulting mechanical properties.

6.1 Future Work

While this work focused on using portable equipment and minimizing processing, future work could be carried out to improve upon the developed procedures. Changes to the processing methods or polymer matrix may be explored to achieve better dispersion and increase mineral filler loading in FDM filaments. While a single screw extruder was used for its portability and low cost, a twin screw extruder or solvent based mixing may lead to improved mechanical properties. Alternatively, formulations of low viscosity polymers have been shown to accommodate higher loadings of filler. Ceramic filler loading well over 50 wt.% has been shown in FDM, although the focus has been aimed toward the manufacture of green bodies, which have poor mechanical properties before sintering [87]–[89]. The use of a polymer matrix with low melt viscosity may allow for better dispersion of filler and further improvements to the mechanical properties of the polymer. As ABS is the most commonly used polymer in FDM and is also used in a wide variety of products, it would also be interesting to study the mechanical properties of recycled ABS/mineral composites and degradation through repeated processing. This would allow for the design of parts utilizing polymer and minerals found *in situ.*

In the creation of ceramics from *in situ* minerals, further work should be conducted to investigate the sintering behavior of unrefined powder and resulting mechanical properties. Variations in particle size distribution, morphology, and chemical composition will influence the

sintering time and temperature needed to form dense structures. Powder processing could also be refined to create more regularly shaped particles, which would allow for increased powder loading and likely lead to higher densities of sintered structures [90]. As furnace sintering is a high energy process, alternative methods should also be explored. Solar furnaces have been demonstrated to be capable of sintering various ceramic powders at temperatures up to 1860°C [91]–[93]. This work provides a pathway for *in situ* resource utilization in additive manufacturing processes carried out in remote environments and establishes the feasibility of using these methods to create complex polymer composite and ceramic structures on demand.

REFERENCES

[1] T. Wohlers and T. Gornet, "History of Additive Manufacturing," in *Wohlers Report 2016*, Boulder: Wohlers Associates, Inc., 2016, pp. 1–38.

[2] ISO/ASTM52900-15, 2015, "Standard Terminology for Additive Manufacturing – General Principles – Terminology," West Conshohocken: ASTM International, 2015.

[3] M. Molitch-Hou, "Overview of additive manufacturing process," in *Additive Manufacturing: Materials, Processes, Quantifications and Applications*, 1st ed., J. Zhang and Y.-G. Jung, Eds. Oxford: Elsevier Inc., 2018, pp. 1–38.

[4] M. P. Snyder, J. J. Dunn, and E. G. Gonzalez, "Effects of Microgravity on Extrusion based Additive Manufacturing," in *AIAA SPACE Conference and Exposition*, 2013, pp. 1–6.

[5] "Space Station 3D-Printer Builds Ratchet Wrench to Complete First Phase of Operations," *NASA*, 2014. [Online]. Available: https://www.nasa.gov/mission_pages/station/research/news/3Dratchet_wrench. [Accessed: 18-Apr-2019].

[6] M. Cox, "Mobile Labs Build On-the-Spot Combat Solutions," *Military.com*, 2012. [Online]. Available: https://www.military.com/daily-news/2012/08/17/mobile-labs-build-on-the-spot-combat-solutions.html. [Accessed: 02-May-2019].

[7] S. Barkley, "Mobile Parts Hospital resuscitate broken gear," *U.S. Army*, 2009. [Online]. Available: https://www.army.mil/article/21502/mobile_parts_hospitals_resuscitate_broken_gear. [Accessed: 02-May-2019].

[8] J. M. Conant, "Army researchers develop cold-spray system, transition to industry," *U.S.*

Army, 2015. [Online]. Available: https://www.army.mil/article/148465/army_researchers_develop_cold_spray_system_tran sition_to_industry. [Accessed: 14-Jun-2019].

[9] "Aussie Metal 3D Printing Company on Global Fast Track," *Spee3d Press Release*, 2019. [Online]. Available: https://www.spee3d.com/2019/06/13/press-release-aussie-metal-3d-printing-company-on-global-fast-track/.

[10] M. I. Mohammed, A. Das, E. Gomez-kervin, D. Wilson, and I. Gibson, "EcoPrinting: Investigating the use of 100% recycled Acrylonitrile Butadiene Styrene (ABS) for Additive Manufacturing," in *Solid Freeform Fabrication Symposium*, 2017, pp. 532–542.

[11] M. S. Pepi, "Advances in Additive Manufacturing," US Army Research Lab, Aberdeen Proving Ground, MD, Rep. no. ARL-SR-0357, July 2016.

[12] N. A. Meisel, C. B. Williams, K. P. Ellis, and D. Taylor, "Decision support for additive manufacturing deployment in remote or austere environments," *J. Manuf. Technol. Manag.*, vol. 27, no. 7, pp. 898–914, 2016.

[13] A. Sgambati *et al.*, "URBAN: conceiving a lunar base using 3D printing technologies," in *International Astronautical Congress*, 2018, no. 69, pp. 1–9.

[14] M. I. Mohammed, D. Wilson, E. Gomez-kervin, C. Vidler, L. Rosson, and J. Long, "The recycling of E-Waste ABS plastics by melt extrusion and 3D printing using solar powered devices as a transformative tool for humanitarian aid," in *Solid Freeform Fabrication Proceedings*, 2018, no. 29, pp. 80–92.

[15] B. J. Chow, T. Chen, Y. Zhong, and Y. Qiao, "Direct Formation of Structural Components Using a Martian Soil Simulant," *Sci. Rep.*, vol. 7, no. 1151, pp. 1–8, 2017.

[16] P. Hintze, J. Curran, and T. Back, "Lunar Surface Stabilization via Sintering or the Use of Heat Cured Polymers," in *47th AIAA Aerospace Sciences Meeting*, 2009.

[17] A. Meurisse, A. Makaya, C. Willsch, and M. Sperl, “Solar 3D printing of lunar regolith,” *Acta Astronaut.*, vol. 152, pp. 800–810, 2018.

[18] G. Cesaretti, E. Dini, X. De Kestelier, V. Colla, and L. Pambaguian, “Building components for an outpost on the Lunar soil by means of a novel 3D printing technology,” *Acta Astronaut.*, vol. 93, pp. 430–450, 2014.

[19] D. Crenshaw *et al.*, “To infinity and beyond: Outer space applications of 3-D ceramics printed via ink jet methods,” *Am. Ceram. Soc. Bull.*, vol. 97, no. 6, pp. 23–28, 2018.

[20] V. K. Balla, L. B. Roberson, G. W. O’Connor, S. Trigwell, S. Bose, and A. Bandyopadhyay, “First demonstration on direct laser fabrication of lunar regolith parts,” *Rapid Prototyp. J.*, vol. 18, no. 6, pp. 451–457, 2012.

[21] A. Goulas, R. A. Harris, and R. J. Friel, “Additive manufacturing of physical assets by using ceramic multicomponent extra-terrestrial materials,” *Addit. Manuf.*, vol. 10, pp. 36–42, 2016.

[22] A. Goulas, J. G. P. Binner, R. A. Harris, and R. J. Friel, “Assessing extraterrestrial regolith material simulants for in-situ resource utilisation based 3D printing,” *Appl. Mater. Today*, vol. 6, pp. 54–61, 2017.

[23] A. E. Jakus, K. D. Koube, N. R. Geisendorfer, and R. N. Shah, “Robust and Elastic Lunar and Martian Structures from 3D-Printed Regolith Inks,” *Sci. Rep.*, vol. 7, pp. 1–8, 2017.

[24] S. L. Taylor *et al.*, “Sintering of micro-trusses created by extrusion-3D-printing of lunar regolith inks,” *Acta Astronaut.*, vol. 143, pp. 1–8, 2018.

[25] “Sending American Astronauts to Moon in 2024: NASA Accepts Challenge,” *NASA*, 2019. [Online]. Available: https://www.nasa.gov/feature/sending-american-astronauts-to-moon-in-2024-nasa-accepts-challenge. [Accessed: 10-May-2019].

[26] E. A. Fisher *et al.*, "Evidence for surface water ice in the lunar polar regions using reflectance measurements from the Lunar Orbiter Laser Altimeter and temperature measurements from the Diviner Lunar Radiometer Experiment," *Icarus*, vol. 292, pp. 74–85, 2017.

[27] M. C. Fuerstenau and K. N. Han, "Introduction," in *Principles of Mineral Processing*, M. Fuerstenau and K. Han, Eds. Littleton: SME, 2003, pp. 1–8.

[28] S. Y. Fu, X. Q. Feng, B. Lauke, and Y. W. Mai, "Effects of particle size, particle/matrix interface adhesion and particle loading on mechanical properties of particulate-polymer composites," *Compos. Part B Eng.*, vol. 39, no. 6, pp. 933–961, 2008.

[29] R. N. Rothon, "Mineral Fillers in Thermoplastics: Filler Manufacture and Characterization," in *Advances in Polymer Science*, J. Jancar, Ed. Berlin: Springer-Verlag, 1999, pp. 67–104.

[30] S. L. Kang, "Basis of Sintering Science," in *Sintering: Densification, grain growth, and microstructure*, Burlington: Elsevier Science and Technology, 2005, pp. 1–36.

[31] O. A. Mohamed, S. H. Masood, and J. L. Bhowmik, "Optimization of fused deposition modeling process parameters: a review of current research and future prospects," *Adv. Manuf.*, vol. 3, no. 1, pp. 42–53, 2015.

[32] X. Wang, M. Jiang, Z. Zhou, J. Gou, and D. Hui, "3D printing of polymer matrix composites: A review and prospective," *Compos. Part B Eng.*, vol. 110, pp. 442–458, 2017.

[33] J. R. Fried, "Additives, Blends, Block Copolymers, and Composites," in *Polymer Science and Technology*, 3rd ed., Upper Saddle River: Pearson Education, Inc., 2014, pp. 281–329.

[34] “Markforged.” [Online]. Available: https://markforged.com/. [Accessed: 11-Aug-2019].

[35] Markforged, “Composites,” Material Datasheet Rev 3.1, May 2019.

[36] “MatterHackers.” [Online]. Available: https://www.matterhackers.com/. [Accessed: 11-Aug-2019].

[37] “Formfutura.” [Online]. Available: https://www.formfutura.com/. [Accessed: 11-Aug-2019].

[38] W. Zhong, F. Li, Z. Zhang, L. Song, and Z. Li, “Short fiber reinforced composites for fused deposition modeling,” *Mater. Sci. Eng. A*, vol. 301, pp. 125–130, 2001.

[39] F. Ning, W. Cong, J. Qiu, J. Wei, and S. Wang, “Additive manufacturing of carbon fiber reinforced thermoplastic composites using fused deposition modeling,” *Compos. Part B Eng.*, vol. 80, pp. 369–378, 2015.

[40] M. L. Shofner, K. Lozano, F. J. Rodriguez-Macias, and E. V. Barrera, “Nanofiber-reinforced polymers prepared by fused deposition modeling,” *J. Appl. Polym. Sci.*, vol. 89, no. 11, pp. 3081–3090, 2003.

[41] X. Wei *et al.*, “3D Printable Graphene Composite,” *Sci. Rep.*, vol. 5, pp. 1–7, 2015.

[42] S. Dul, L. Fambri, and A. Pegoretti, “Fused deposition modelling with ABS-graphene nanocomposites,” *Compos. Part A Appl. Sci. Manuf.*, vol. 85, pp. 181–191, 2016.

[43] Z. Weng, J. Wang, T. Senthil, and L. Wu, “Mechanical and thermal properties of ABS/montmorillonite nanocomposites for fused deposition modeling 3D printing,” *Mater. Des.*, vol. 102, pp. 276–283, 2016.

[44] B. Coppola, N. Cappetti, L. Di Maio, P. Scarfato, and L. Incarnato, “3D printing of PLA/clay nanocomposites: Influence of printing temperature on printed samples properties,” *Materials*, vol. 11, no. 10, pp. 1–17, 2018.

[45] “Lay-filaments.” [Online]. Available: http://lay-filaments.com/. [Accessed: 11-Aug-2019].

[46] “colorFabb.” [Online]. Available: https://colorfabb.com. [Accessed: 11-Aug-2019].

[47] “Proto-pasta.” [Online]. Available: https://www.proto-pasta.com/. [Accessed: 11-Aug-2019].

[48] Formfutura, “StoneFil™,” Technical Data Sheet v3, 2019.

[49] B. M. Tymrak, M. Kreiger, and J. M. Pearce, “Mechanical properties of components fabricated with open-source 3-D printers under realistic environmental conditions,” *Mater. Des.*, vol. 58, pp. 242–246, 2014.

[50] M. Nikzad, S. H. Masood, and I. Sbarski, “Thermo-mechanical properties of a highly filled polymeric composites for Fused Deposition Modeling,” *Mater. Des.*, vol. 32, no. 6, pp. 3448–3456, 2011.

[51] K. Boparai, R. Singh, and H. Singh, “Comparison of tribological behaviour for Nylon6-Al-Al2O3 and ABS parts fabricated by fused deposition modelling,” *Virtual Phys. Prototyp.*, vol. 10, no. 2, pp. 59–66, 2015.

[52] D. V. Isakov, Q. Lei, F. Castles, C. J. Stevens, C. R. M. Grovenor, and P. S. Grant, “3D printed anisotropic dielectric composite with meta-material features,” *Mater. Des.*, vol. 93, pp. 423–430, 2016.

[53] F. Castles *et al.*, “Microwave dielectric characterisation of 3D-printed BaTiO3/ABS polymer composites,” *Sci. Rep.*, vol. 6, no. March, pp. 1–8, 2016.

[54] C. M. Shemelya *et al.*, “Mechanical, Electromagnetic, and X-ray Shielding Characterization of a 3D Printable Tungsten–Polycarbonate Polymer Matrix Composite for Space-Based Applications,” *J. Electron. Mater.*, vol. 44, no. 8, pp. 2598–2607, 2015.

[55] S. Woosley, N. Abuali Galehdari, A. Kelkar, and S. Aravamudhan, “Fused deposition

modeling 3D printing of boron nitride composites for neutron radiation shielding," *J. Mater. Res.*, vol. 33, no. 22, pp. 3657–3664, 2018.

[56] S. J. Kalita, S. Bose, H. L. Hosick, and A. Bandyopadhyay, "Development of controlled porosity polymer-ceramic composite scaffolds via fused deposition modeling," *Mater. Sci. Eng. C*, vol. 23, no. 5, pp. 611–620, 2003.

[57] A. R. Torrado, C. M. Shemelya, J. D. English, Y. Lin, R. B. Wicker, and D. A. Roberson, "Characterizing the effect of additives to ABS on the mechanical property anisotropy of specimens fabricated by material extrusion 3D printing," *Addit. Manuf.*, vol. 6, pp. 16–29, 2015.

[58] M. R. Skorski, J. M. Esenther, Z. Ahmed, A. E. Miller, and M. R. Hartings, "The chemical, mechanical, and physical properties of 3D printed materials composed of TiO2-ABS nanocomposites," *Sci. Technol. Adv. Mater.*, vol. 17, no. 1, pp. 89–97, 2016.

[59] D. Arencón and J. I. Velasco, "Fracture toughness of polypropylene-based particulate composites," *Materials*, vol. 2, no. 4, pp. 2046–2094, 2009.

[60] N. Venkataraman *et al.*, "Feedstock material property – process relationships in fused deposition of ceramics (FDC)," *Rapid Prototyp. J.*, vol. 6, no. 4, pp. 244–253, 2000.

[61] J. Cesarano, "A Review of Robocasting Technology," *MRS Proc.*, vol. 542, pp. 133–139, 1999.

[62] E. Feilden, E. G. T. Blanca, F. Giuliani, E. Saiz, and L. Vandeperre, "Robocasting of structural ceramic parts with hydrogel inks," *J. Eur. Ceram. Soc.*, vol. 36, no. 10, pp. 2525–2533, 2016.

[63] E. Peng, D. Zhang, and J. Ding, "Ceramic Robocasting: Recent Achievements, Potential, and Future Developments," *Adv. Mater.*, vol. 30, no. 1802404, pp. 1–14, 2018.

[64] J. Franco, P. Hunger, M. E. Launey, A. P. Tomsia, and E. Saiz, “Direct write assembly of calcium phosphate scaffolds using a water-based hydrogel,” *Acta Biomater.*, vol. 6, no. 1, pp. 218–228, 2010.

[65] E. Peng *et al.*, “Robocasting of dense yttria-stabilized zirconia structures,” *J. Mater. Sci.*, vol. 53, no. 1, pp. 247–273, 2018.

[66] “Planetary Simulant Database: LMS-1 Lunar Mare Simulant.” [Online]. Available: https://sciences.ucf.edu/class/simulant_lunarmare/. [Accessed: 15-July-2019].

[67] B. Marler, “On the Relationship between Refractive Index and Density for SiO2-polymorphs,” *Phys. Chem. Miner.*, vol. 16, pp. 286–290, 1988.

[68] D. D. Dabrowska, O. Muñoz, F. Moreno, J. L. Ramos, J. Martínez-Frías, and G. Wurm, “Scattering matrices of martian dust analogs at 488nm and 647nm,” *Icarus*, vol. 250, pp. 83–94, 2015.

[69] E. A. King, J. C. Butler, and M. F. Carman, “The lunar regolith as sampled by Apollo 11 and Apollo 12: Grain size analyses, modal analyses, and origins of particles,” in *Second Lunar Science Conference*, 1971, vol. 1, pp. 737–746.

[70] K. G. J. Christiyan, U. Chandrasekhar, and K. Venkateswarlu, “A study on the influence of process parameters on the Mechanical Properties of 3D printed ABS composite,” in *IOP Conference Series: Materials Science and Engineering*, 2016, vol. 114, pp. 1–8.

[71] B. N. Turner, R. Strong, and S. A. Gold, “A review of melt extrusion additive manufacturing processes: I. Process design and modeling,” *Rapid Prototyp. J.*, vol. 20, no. 3, pp. 192–204, 2014.

[72] A. Ranellucci, “Slic3r: Open source 3D printing toolbox.” [Online]. Available: slic3r.org. [Accessed: 10-July-2019].

[73] Z. C. Chen, K. Ikeda, T. Murakami, and T. Takeda, “Effect of particle packing on extrusion behavior of pastes,” *J. Mater. Sci.*, vol. 35, pp. 5301–5307, 2000.

[74] J. Jiang *et al.*, “Rheology of Thermoreversible Hydrogels from Multiblock Associating Copolymers,” *Macromolecules*, vol. 41, pp. 3646–3652, 2008.

[75] “Ultimaker Cura.” [Online]. Available: https://ultimaker.com/software/ultimaker-cura. [Accessed: 10-July-2019].

[76] D. H. Droste and A. T. Dibenedetto, “The glass transition temperature of filled polymers and its effect on their physical properties,” *J. Appl. Polym. Sci.*, vol. 13, pp. 2149–2168, 1969.

[77] ASTM Standard D638, 2014, “Standard test method for tensile properties of plastics,” 2014. West Conshohocken: ASTM International, 2015.

[78] O. S. Es-Said, J. Foyos, R. Noorani, M. Mendelson, R. Marloth, and B. A. Pregger, “Effect of Layer Orientation on Mechanical Properties of Rapid Prototyped Samples,” *Mater. Manuf. Process.*, vol. 15, no. 1, pp. 107–122, 2000.

[79] L. Engel, H. Klingele, G. W. Ehrenstein, and H. Schaper, *An Atlas of Polymer Damage: Surface examination by scanning electron microscope*. London: Society of Chemical Industry, 1981.

[80] B. Arkles, Y. Pan, G. L. Larson, and D. H. Berry, “Cyclic azasilanes: volatile coupling agents for nanotechnology,” *Silanes and Other Coupling Agents*, vol. 3, pp. 179–191, 2004.

[81] M. Z. Rong, M. Q. Zhang, and W. H. Ruan, “Surface modification of nanoscale fillers for improving properties of polymer nanocomposites: a review,” *Mater. Sci. Technol.*, vol. 22, no. 7, pp. 787–796, 2006.

[82] Y. G. E. V Hsu and F. J. Lin, “Organic-Inorganic Composite Materials from Acrylonitrile-Butadiene-Styrene Copolymers (ABS) and Silica through an In Situ Sol-Gel Process,” *J. Appl. Polym. Sci.*, vol. 75, pp. 275–283, 2000.

[83] I. J. Kim, O. S. Kwon, J. B. Park, and H. Joo, “Synthesis and characterization of ABS/silica hybrid nanocomposites,” *Curr. Appl. Phys.*, vol. 6, no. 1, pp. 43–47, 2006.

[84] L. Jiang, Y. C. Lam, K. C. Tam, T. H. Chua, G. W. Sim, and L. S. Ang, “Strengthening acrylonitrile-butadiene-styrene (ABS) with nano-sized and micron-sized calcium carbonate,” *Polymer*, vol. 46, pp. 243–252, 2005.

[85] M. Hancock, “Filled thermoplastics,” in *Particulate-Filled Polymer Composites*, R. Rothon, Ed. New York: Longman Group Limited, 1995, pp. 279–314.

[86] Q. Fu, E. Saiz, and A. P. Tomsia, “Direct ink writing of highly porous and strong glass scaffolds for load-bearing bone defects repair and regeneration,” *Acta Biomater.*, vol. 7, no. 10, pp. 3547–3554, 2011.

[87] N. Venkataraman *et al.*, “Mechanical Properties Of Feedstock Material For Fused Deposition Of Ceramics,” in *Mat. Res. Soc. Symp. Proc.*, 1999, vol. 542, pp. 111–117.

[88] T. F. McNulty, F. Mohammadi, A. Bandyopadhyay, D. J. Shanefield, S. C. Danforth, and A. Safari, “Development of a binder formulation for fused deposition of ceramics,” *Rapid Prototyp. J.*, vol. 4, no. 2–4, pp. 144–150, 1998.

[89] S. Onagoruwa, S. Bose, and A. Bandyopadhyay, “Fused deposition of ceramics (FDC) and composites,” in *Proceedings of Solid Freeform Fabrication Symposium*, 2001, pp. 224–231.

[90] D. M. Liu, “Particle packing and rheological property of highly-concentrated ceramic suspensions: φm determination and viscosity prediction,” *J. Mater. Sci.*, vol. 35, pp.

5503–5507, 2000.

[91] F. A. C. Oliveira, N. Shohoji, J. C. Fernandes, and L. G. Rosa, “Solar sintering of cordierite-based ceramics at low temperatures,” *Sol. Energy*, vol. 78, no. 3, pp. 351–361, 2005.

[92] R. Román, I. Cañadas, J. Rodríguez, M. T. Hernández, and M. González, “Solar sintering of alumina ceramics: Microstructural development,” *Sol. Energy*, vol. 82, no. 10, pp. 893–902, 2008.

[93] Y. Zhydachevskii *et al.*, “Solid-state and solar sintering of YAP:Mn,Hf ceramics applicable for thermoluminescent dosimetry,” *Opt. Mater.*, vol. 45, pp. 246–251, 2015.